Final Technical Report

Project Title: Sustainable Energy Solutions
Task 4.1 Intelligent Manufacturing of Hybrid Carbon-Glass Fiber-Reinforced Composite Wind Turbine Blades
Award Number: DE-FG36-08GO88149
Recipient: Wichita State University

Project Location(s): Wichita State University
Wichita, Kansas 67260

Project Period: June 1, 2008 – December 31, 2009
Date of Report: *March 1, 2010*
Written by: Bob Minaie, Ph.D.

Program Manager:
Debbie Weems
Technical Project Officer
Inventions and Innovations Program
United States Department of Energy
Golden Office
1617 Cole Boulevard
Golden, CO 80401-3393
Principal Investigators:

Subcontractors:

Cost-Sharing Partners: Wichita State University

Acknowledgment: This material is based upon work supported by the Department of Energy under Award Number DE-FG36-08GO88149.

FINAL TECHNICAL REPORT

Sustainable Energy Solutions

DE-FG36-08GO88149

Task 4.1

Intelligent Manufacturing of Hybrid Carbon-Glass Fiber-Reinforced Composite Wind Turbine Blades

Project Director

Bob Minaie, Ph.D.

Associate Professor, Mechanical Engineering

WICHITA STATE UNIVERSITY

Wichita, Kansas

PI: Janet M. Twomey, Ph.D.
Professor, Industrial and Manufacturing Engineering

EXECUTIVE SUMARY

In this subtask, the manufacturability of hybrid carbon-glass fiber-reinforced composite wind turbine blades using Vacuum-Assisted Resin Transfer Molding (VARTM) was investigated. The objective of this investigation was to study the VARTM process and its parameters to manufacture cost-effective wind turbine blades with no defects (mainly eliminate dry spots and reduce manufacturing time). A 2.5-dimensional model and a 3-dimensional model were developed to simulate mold filling and part curing under different conditions. These conditions included isothermal and non-isothermal filling, curing of the part during and after filling, and placement of injection gates at different locations. Results from this investigation reveal that the process can be simulated and also that manufacturing parameters can be optimized to eliminate dry spot formation and reduce the manufacturing time.

Using computer-based models is a cost-effective way to simulate manufacturing of wind turbine blades. The approach taken herein allows the design of the wind blade manufacturing processes without physically running trial-and-error experiments that are expensive and time-consuming; especially for larger blades needed for more demanding environmental conditions. This will benefit the wind energy industry by reducing initial design and manufacturing costs which can later be passed down to consumers and consequently make the wind energy industry more competitive.

Comparison of the Actual Accomplishments with the Goals and Objectives of the Project

The College of Engineering (CoE) at Wichita State University (WSU) has engaged in research and development in the area of wind energy, drawing from advances in technology from the aerospace and power systems industries, and expertise in life cycle analysis. The ***overall objective*** of the proposed effort has been to advance the economy of Kansas through the creation of new knowledge of energy production and products for the advancement of wind energy systems. The impediments to more economical and efficient wind energy systems targeted by this effort include the following: lack of access and integration of sustainable energy technologies (wind) into existing energy infrastructure, high cost of wind energy due to low reliability and high cost of wind-turbine maintenance, and lack of quantifiable environmental impact information. The WSU research addresses those impediments and meets the technology barriers to wind energy identified by the Wind and Hydropower Technologies Program, Department of Energy (Wind Energy Multiyear Program Plan for 2007–2012). Through this award, a CoE consortium of wind energy researchers has been created to provide advice to industry and policy makers, educate students, and offer a portal for information exchange.

To meet the overall objective, five specific goals were pursued. This Final Technical Report addresses one specific goal:

To improve the durability of turbine blades through new materials: hybrid carbon-glass composite blades.

The goal of Subtask 4.1 is to improve the manufacturability of carbon-glass fiber-reinforced composite blades. This task is significant because carbon-glass fiber-reinforced composite is more durable than the more common blade materials. Improved manufacturing processes are needed to make carbon-glass fiber-reinforced composite economical. The approach was to utilize mold filling and curing simulation to optimize the manufacturing process parameters using cost-effective vacuum-assisted resin transfer molding (VARTM). The objective of the flow simulation is to eliminate or significantly reduce defect formation. A finite element model capable of handling various blade geometries was used to effectively simulate the filling. This resulted in an effective utilization of resin-dispensing equipment, and the manufacturing process was optimized to produce defect-free blades.

Summary Project Activities

The deliverables for this one year project are as follows:

1. *Simulate the resin-filling pattern during VARTM manufacturing of the wind* blades, which will enable intelligent design of the manufacturing process.
2. Simulate the cure to determine temperature gradients in the composite during this process, which will allow designers to assure structural integrity of the wind blade based on the temperature differences along the part.
3. Optimize parameters for the manufacturing of the wind blades, which include (but are not limited to) the following: gate and vent locations, flow pattern, distribution media placement, and energy requirements.
4. Simulate non-isothermal filling and curing in 3D to determine the best practices during manufacturing of composite blades. This will allow a more realistic simulation of the actual blade fabrication.
5. Parametric study of 3D non-isothermal filling and curing to optimize manufacturing process parameters.

Products Developed and Technology Transfer

A. Publications (Journals, Conference Proceedings, Abstracts, Presentations, Thesis, Dissertation, Student Projects)
   - Presentation: Wind Energy Research Symposium, March 26th, 2009, Wichita, KS.
   - M.S. Thesis: Manufacturability of Hybrid Wind Turbine Blades, Wichita State University, to be completed in spring 2010.

B. Web site / Internet sites
   The project website is: www.wichita.edu/sustainability

C. Networks or collaborations fostered;
   - Mr. Scott Hughes, Research Engineer, National Renewable Energy Laboratory (NREL).
   - Dr. Michael Meador, Polymer Branch Chief, NASA Glenn Research Center.
   - Mr. Jose Zayas, Wind Energy Department Manager, Sandia National Laboratories.
   - Mr. Thomas Ashwill, Wind Energy Department Manager, Sandia National Laboratories.
   - Dr. Kyle Wetzel, CEO, Wetzel Engineering.

D. Other products, such as data or databases, physical collections, audio or video, software or netware, models, educational aid or curricula, instruments or equipment.
   - A 2.5-dimensional model for simulating resin infusion and curing in a 48 meters long blade.
   - A 3-dimensional model for simulating resin infusion and curing in a 48 meters long blade.

Computer Model Results

Chapter 1: Isothermal Filling Pattern

Wind Turbine Blade Geometry and Mesh

CATIA was used for creating the geometry and the mesh. The outer surface of the shell was created by multiple airfoil cross-sections along the blade shell, and then the "multi-section surface" function was used to create a smooth surface that passes through all cross sections.

Having a general idea about the shape and the positioning of inlet gates and vents has a great influence on how the elements should be arranged in the surface mesh. During manufacturing of the wind turbine blade, the inlet gates are usually made of several omega-shape channels that are located on top of the part in the longitudinal direction along the blade. Their function is to carry the resin along the length of the blade.

In this simulation, the idea is to align the elements in the same manner so that each strip of elements can be defined as an inlet channel. In order to arrange the elements, guiding curves need to be created. The center guiding curve was created with geodesic center points of the blade's cross-sections in several places by using "spline" function. The rest of the curves are simply offsets from the center curve with 10 cm distance from each other (see Figure 1).

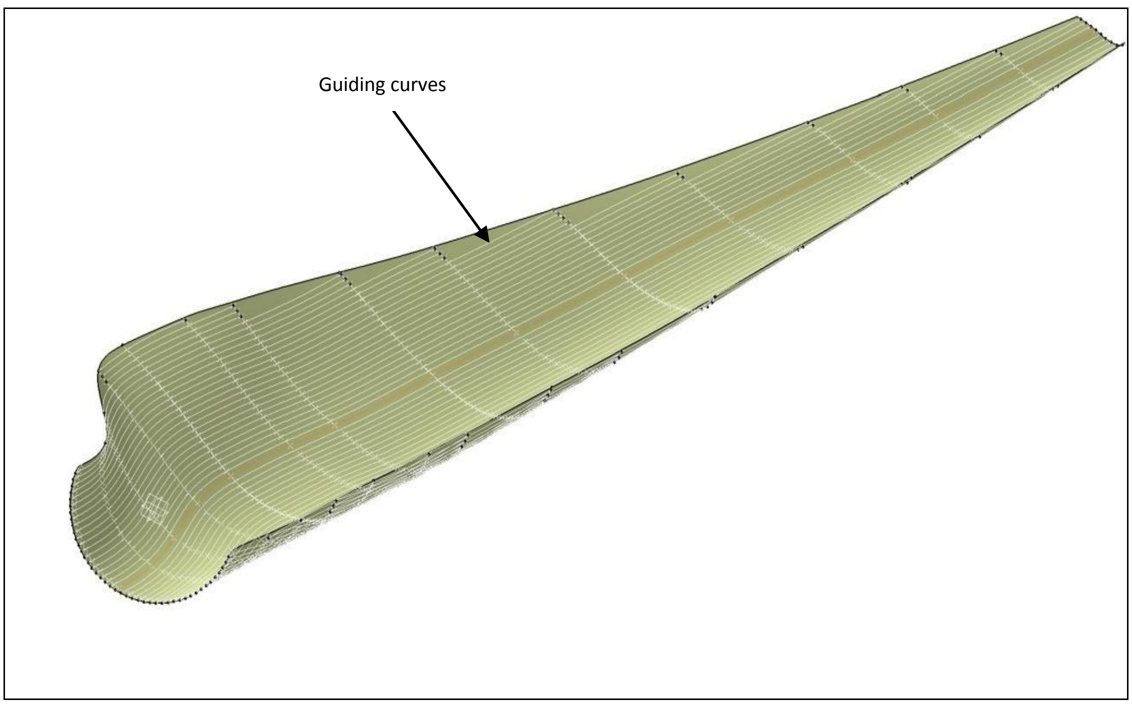

Figure 1. Guiding curves for element arrangement.

The geometry was then imported to the "Advanced Meshing Tool" module for meshing. The location of the nodes needed to be initiated on the guiding curves before meshing function could take place. This was done by using "Impose Elements" function. For the distance between the nodes was 10 cm (see Figure 2).

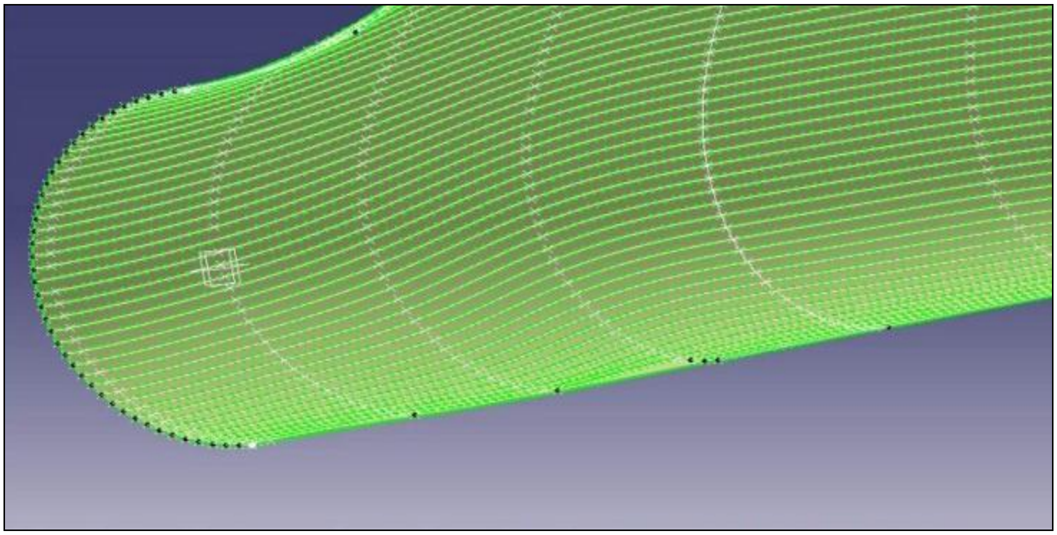

Figure 2. Imposed nodes.

Once the location of the imposed nodes was identified, "Octree Triangle Mesh" function was applied to the surface geometry to discretize it (see Figure 3). The surface mesh was exported as a NASTRAN mesh file to PAM-RTM for 3D mesh extrusion and filling simulation.

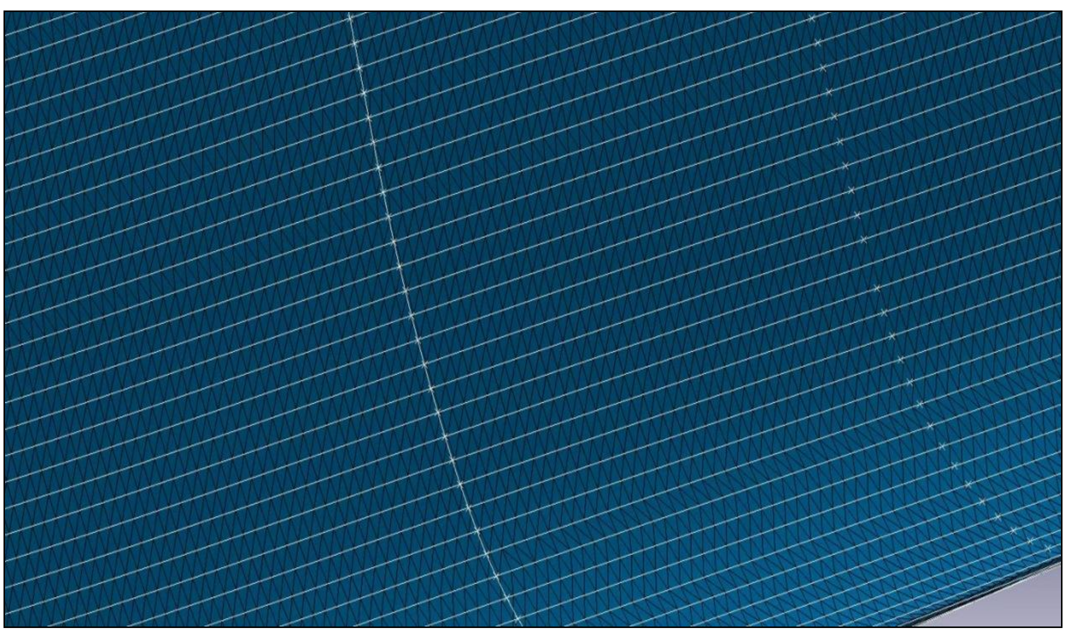

Figure 3. Surface mesh.

Filling Pattern Simulations

Material Properties

The material properties were defined as follows:

Resin

The resin was assumed to be non-thixotropic and isothermal during filling. In theory, curing is initiated from the moment the catalyst is mixed with the resin. However, in order to avoid an increase in resin viscosity during filling, chemicals are added to keep the resin isothermal for 1-2 hours. As such, it is reasonable to assume viscosity and temperature to be constant during filling.

For the resin system, the following properties were used:

- Density: 1000 kg/m^3
- Viscosity: 0.1 Pa.S

Reinforcement Fibers

The preform was made by laying and draping different layers of materials. The compressibility of fibers was neglected and three different materials were used as follows:

- One layer of Continuous Fiber Mat (CFM) on the top and one layer of CFM at the bottom each having a thickness of 1 cm.
- One layer of core material with a thickness of 2 cm.
- One layer of biaxial fiber with a thickness of 1 cm in sandwich areas and a thickness of 2 cm in other areas.

The permeability orientation for all the fibers are defined as K_1 in the longitudinal direction of the blade, K_2 is perpendicular to K_1, and K_3 in the through-thickness direction. Permeability values are shown below.

- CFM $K_1 = K_2 = K_3 = 1\times10^{-8}\ m^2$
- Biaxial $K_1 = K_2 = 1\times10^{-9}\ m^2$, $K_3 = 1\times10^{-11}\ m^2$

Mesh Extrusion

The “Mesh Extrusion” function was then used to create six node pentahedral elements with respect to layer thicknesses. Figure 4 illustrates how the layers of the fiber and the core material were positioned.

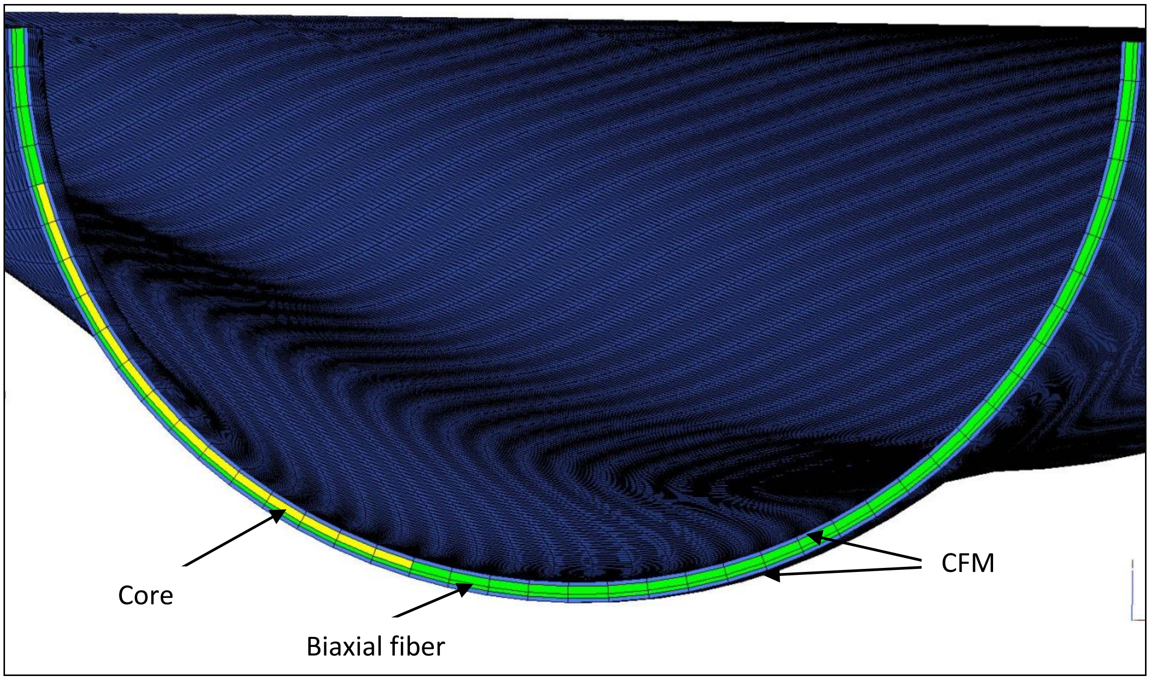

Figure 4. Cross-section of the discretized composite wind turbine blade.

Inlet Gate and Vents Location

The inlet was defined on the elements located on the center curve of the shell. The inlet is shown as a green strip in Figure 5. The exit vents were placed on the edges of the shell that were assumed to be the locations of the last point to fill. The exit vents are shown in red color in Figure 5. The pressure at the inlet gate was assumed to be constant with a value of 1.06×10^{5} MPa and the pressure at the exit vents was assumed to be zero.

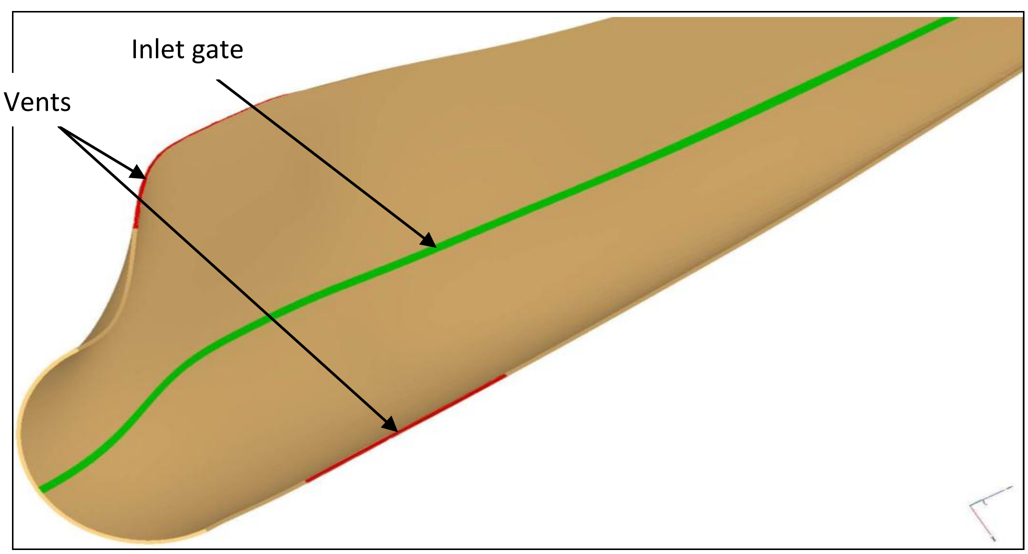

Figure 5. Location of inlet gate and exit vents.

Results for Filling Pattern Simulations

The filling pattern simulations are shown in Figures 6-8.

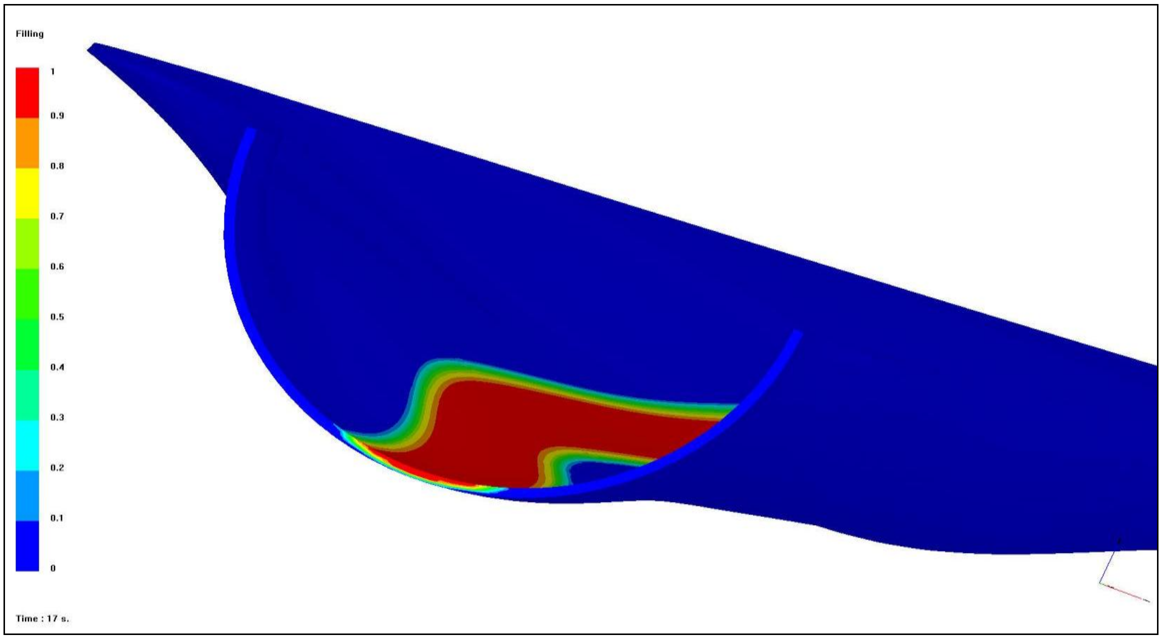

Figure 6. Filling pattern at t=17 s.

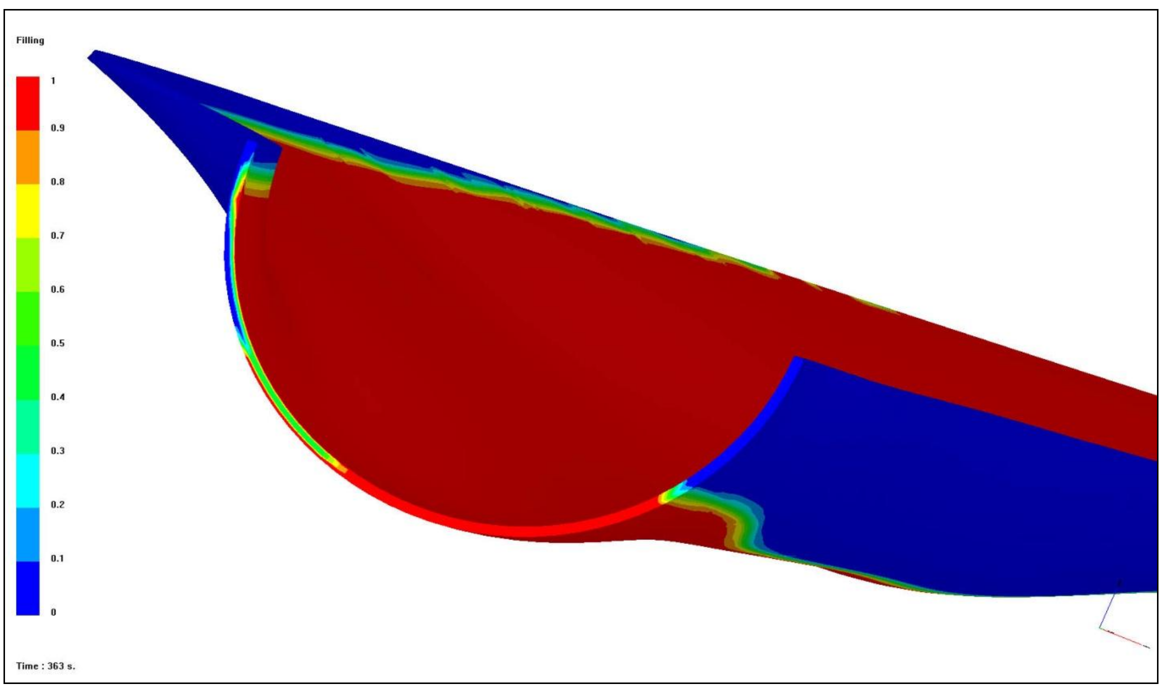

Figure 7. Filling pattern at t=363 s.

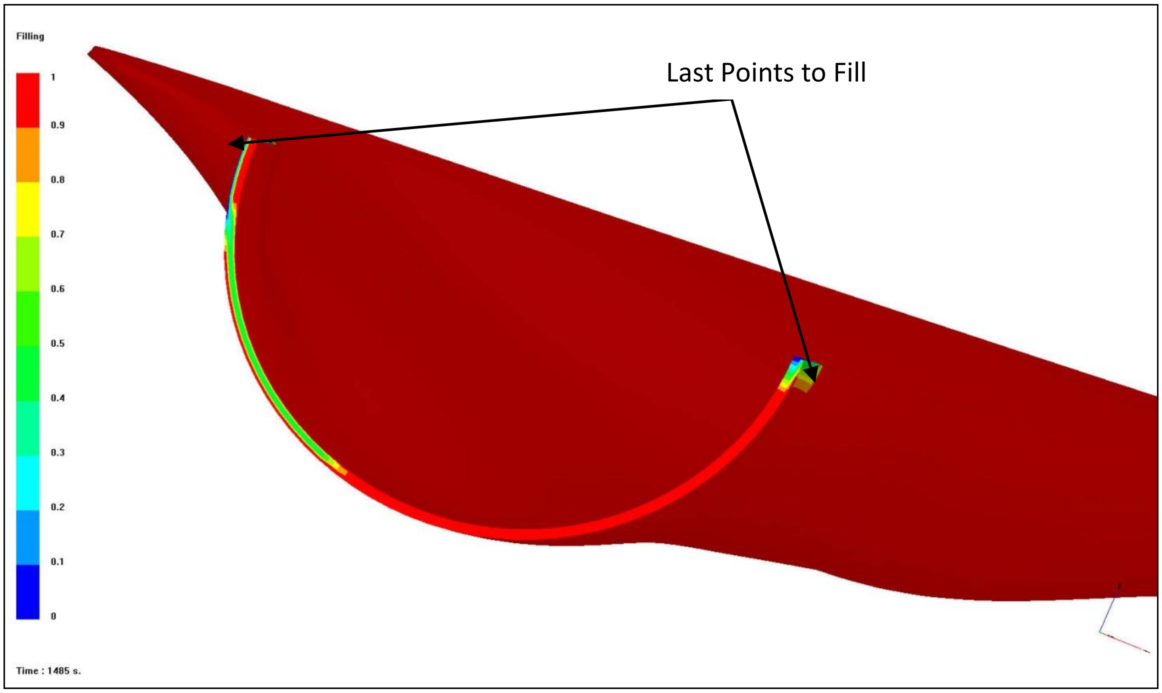

Figure 8. End of filling showing the last points to fill at t=1485 s.

Figure 9 shows the dry spots at the corners of the blade root.

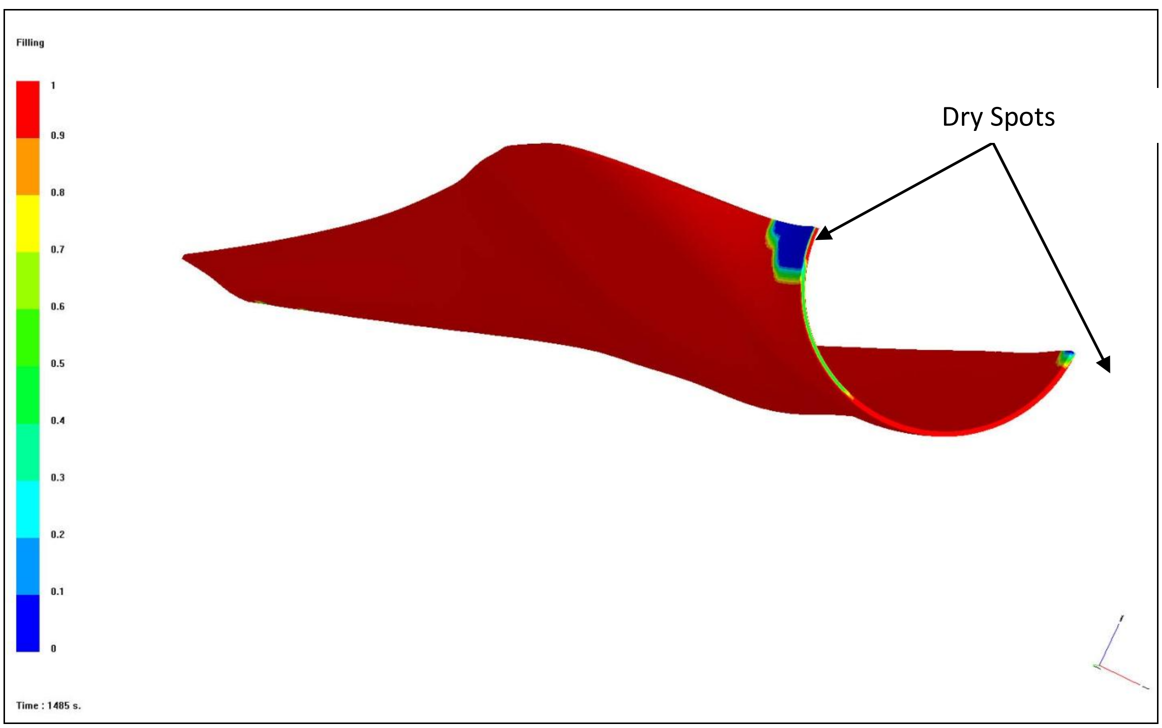

Figure 9. Dry spots.

Pressure distribution during the filling is shown in Figures 10-12.

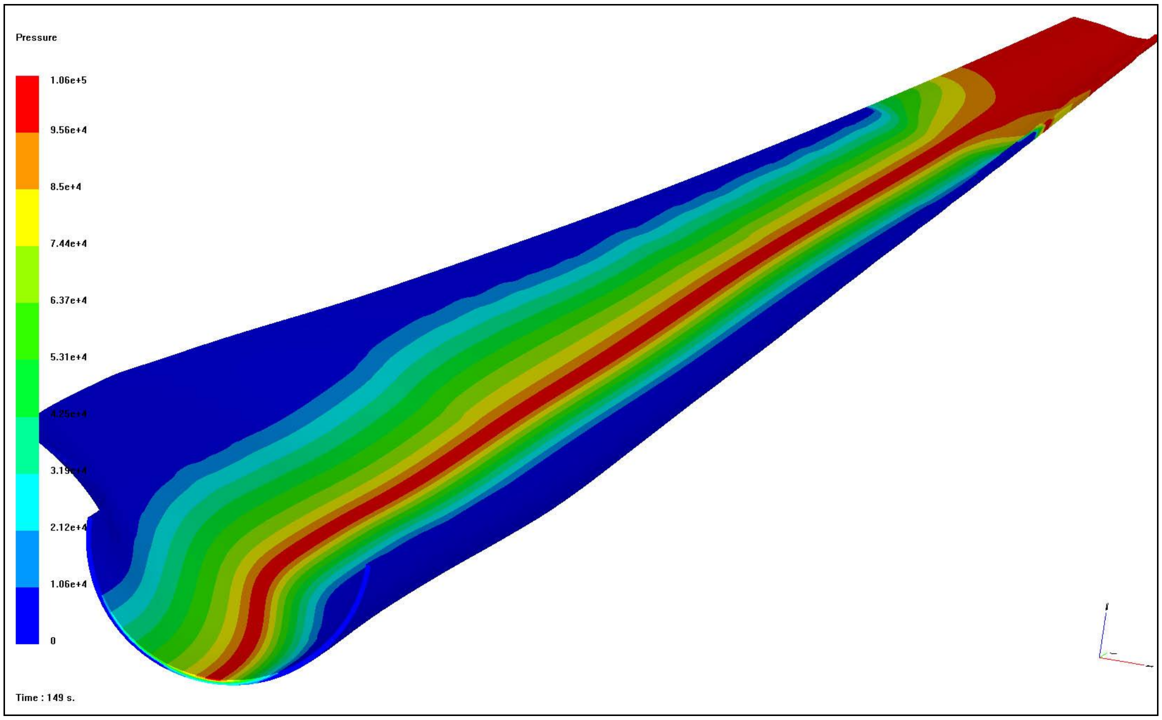

Figure 10. Pressure distribution at t=149 s.

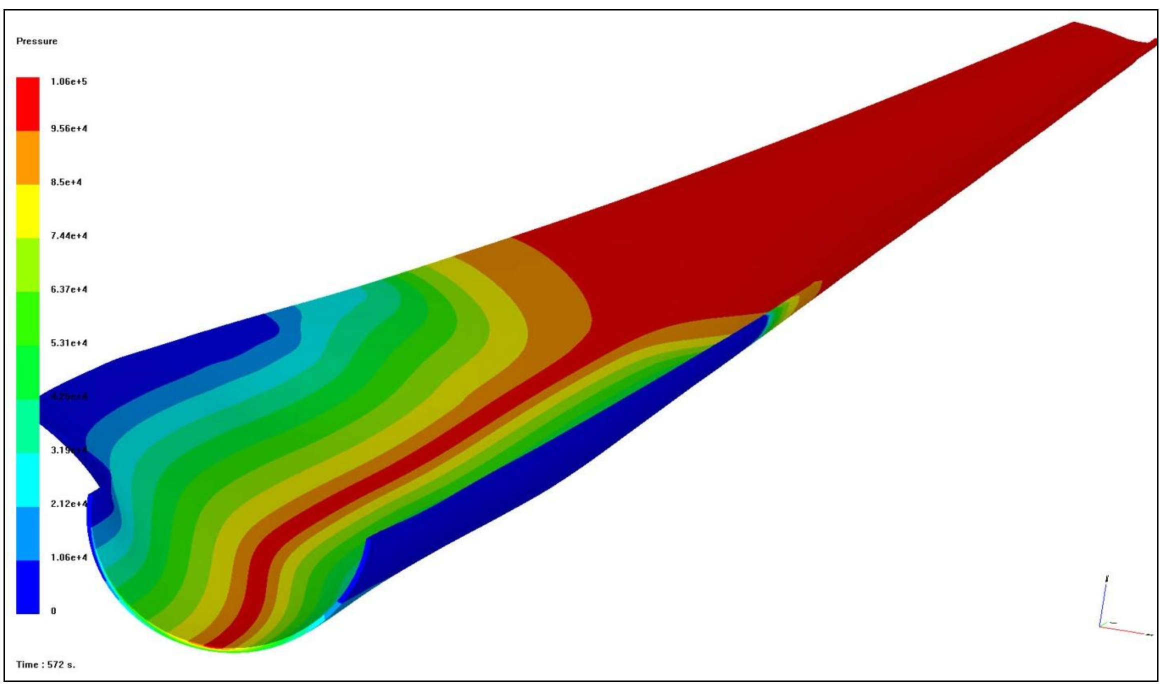

Figure 11. Pressure distribution at t=572 s.

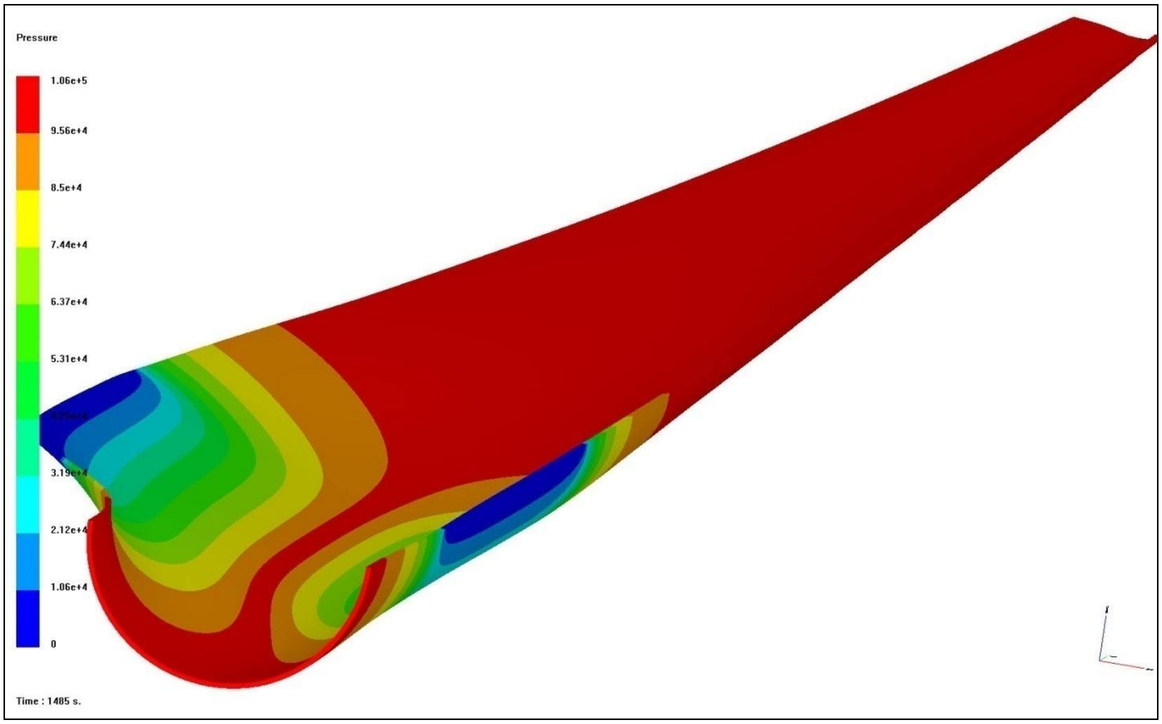

Figure 12. Pressure distribution at the end of filling at t=1485 s.

Chapter 2: Curing after Isothermal Filling

Curing Simulation after Isothermal Filling

Kinetic Model for Polymerization

The major assumption for the curing simulation presented in this report is that the cure state of the resin is the same at all points when the curing simulation starts. As such, the time required to infuse the resin has no effect on the degree of cure of the resin.

The model selected to simulate the curing kinetics was the Kamal-Sourour model. The Kamal-Sourour equation for a resin with *n* components is as follows:

$$\alpha = \sum_{i=1}^{n} c_i \; \alpha_i$$

$$\frac{d\alpha_i}{dt} = K_i\,(T).\alpha^{m}{}_{i}.(1-\alpha)^{p}{}_{i}$$

where α is the degree of cure, C_i is the weight parameter of each reaction, K_i is the rate constant of the chemical reaction and $\frac{d\alpha_i}{dt}$ is the rate of reaction for the i[th] component, the values of K_i are defined by the Arrhenius rate law:

$$K_i = A_i \exp\left(-\frac{E_i}{R \cdot T}\right)$$

where A_i are the pre-exponential factors, E_i are the activation energies of the chemical reaction, m_i and p_i are exponents that characterize the sensitivity of each autocatalytic reaction, R is the universal gas constant, and T is the temperature of the system.

Thermal Properties and Boundary Conditions

The initial temperatures for the infused preform and the surrounding air were 295 K and 300 K, respectively. The generated heat from the chemical reaction is transferred by conduction through the part and also convection with the surrounding air. The mold was assumed to have no heating or cooling capabilities. The areas closer to the edges and tip of the blade were assumed to have a higher heat-transfer coefficient than that of the center of the blade (see Figure13).

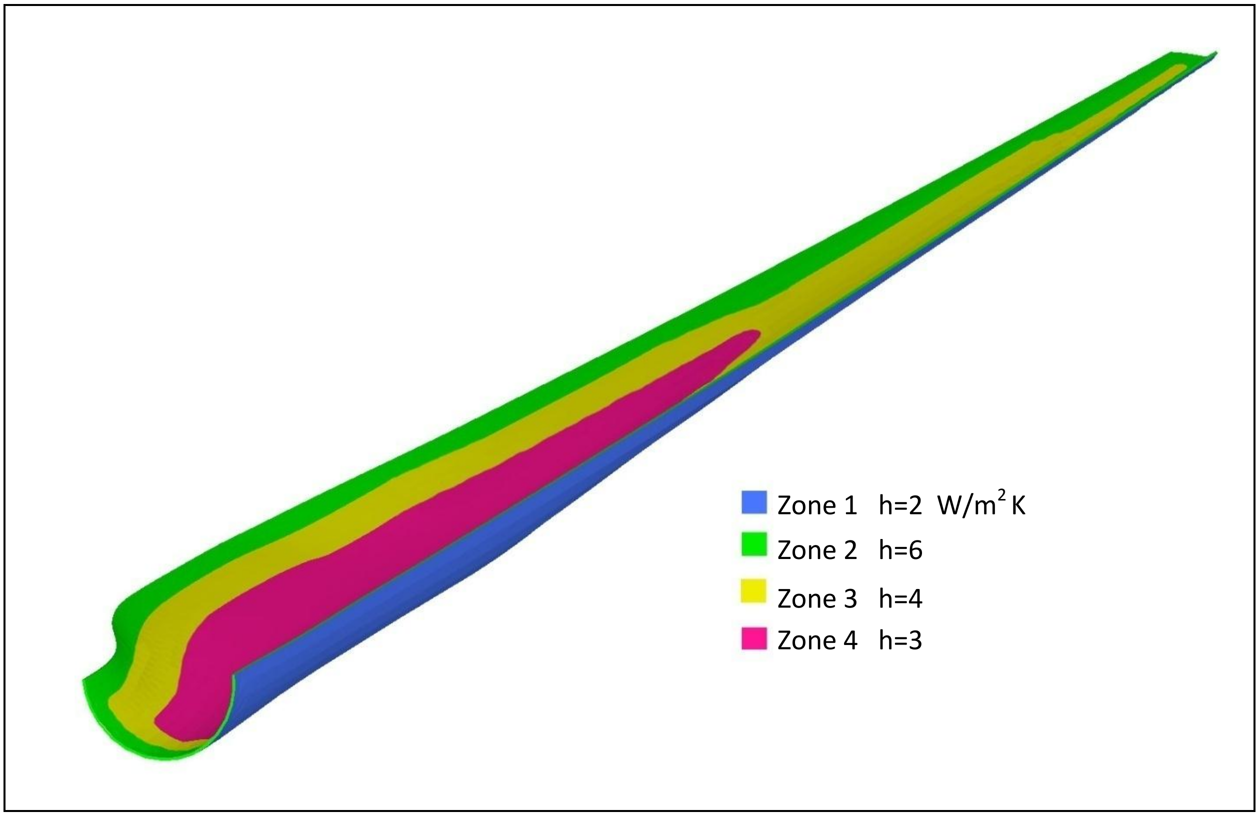

Figure 13. Convection heat transfer coefficient.

The thermal properties of the resin used in this simulation are as follows:

- Pre-exponential factor $A = 1.5 \times 10^4\ s^{-1}$
- Activation energy $\frac{E}{R} = 5.45 \times 10^3$ K
- First exponent m = 0.7
- Second exponent p = 1.3
- Enthalpy of reaction H_r= 142000 J/Kg
- Density ρ_r= 1083 Kg/m^3
- Specific heat C= 1300 J/Kg.K

The following thermal properties were used for the reinforcement:

- Thermal conductivity 0.2 W/m.K
- Effective conductivity 0.3 W/m.K
- Specific heat 1,205 J/Kg.K
- Density 2,565 Kg/m^3

Results for Curing Simulations after Isothermal Filling

The simulations for degree of cure after isothermal filling are shown in Figures 14-17. From these figures, it can be seen that as the simulation starts, the edges are the first areas to begin curing. This is due to their high heat transfer coefficient. As a result, they reach room temperature (initially 5 K higher) and initial cure prior to other areas inside the blade. (Since all the resin has the same initial cure state everywhere, the difference in time at which the resin starts curing on the edges compared to the inside of the blade is not significant.) As time progresses, the resin inside the blade starts to cure and two areas along the longitudinal direction, separated by the core of the blade, can be clearly distinguished. Interestingly, both areas cure in a similar pattern: from the center of each area to the edges of the area. This behavior comes as a result of having the sandwich core located at the middle of the part and, therefore, since the core is not permeable, then there is no resin inside to generate heat. In Figures 14-17, the core area can be distinguished by its relatively lower degree of cure and temperature through-out curing.

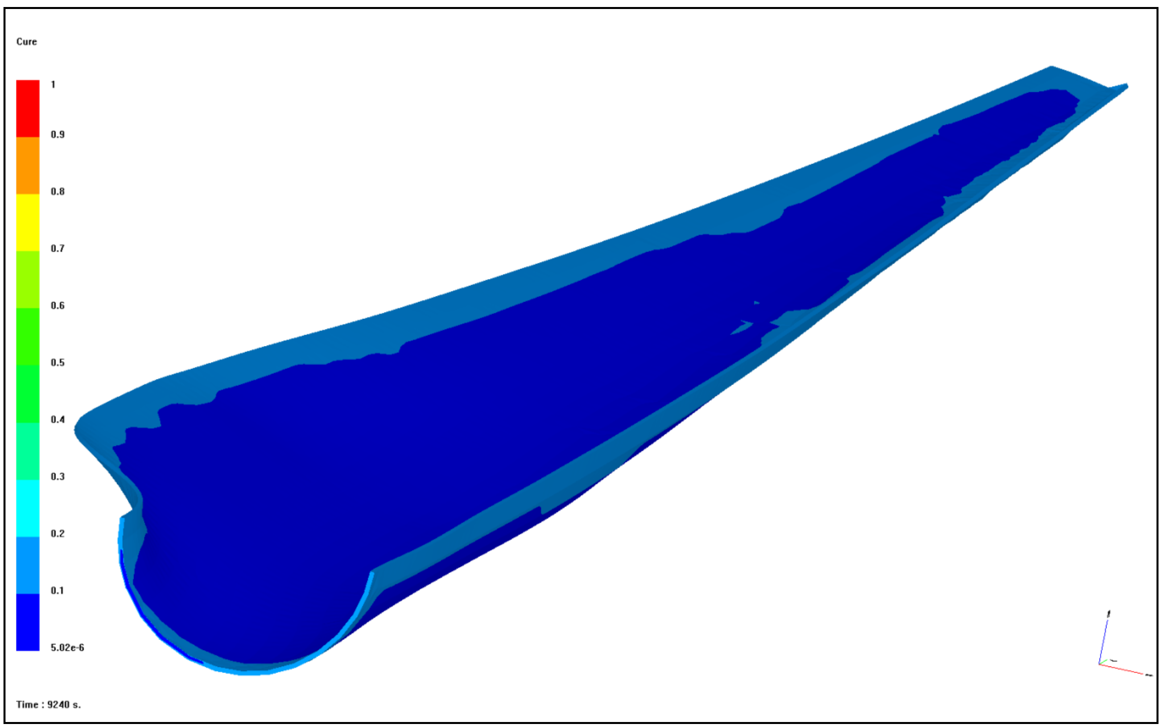

Figure 14. Degree of cure at 9,240 s.

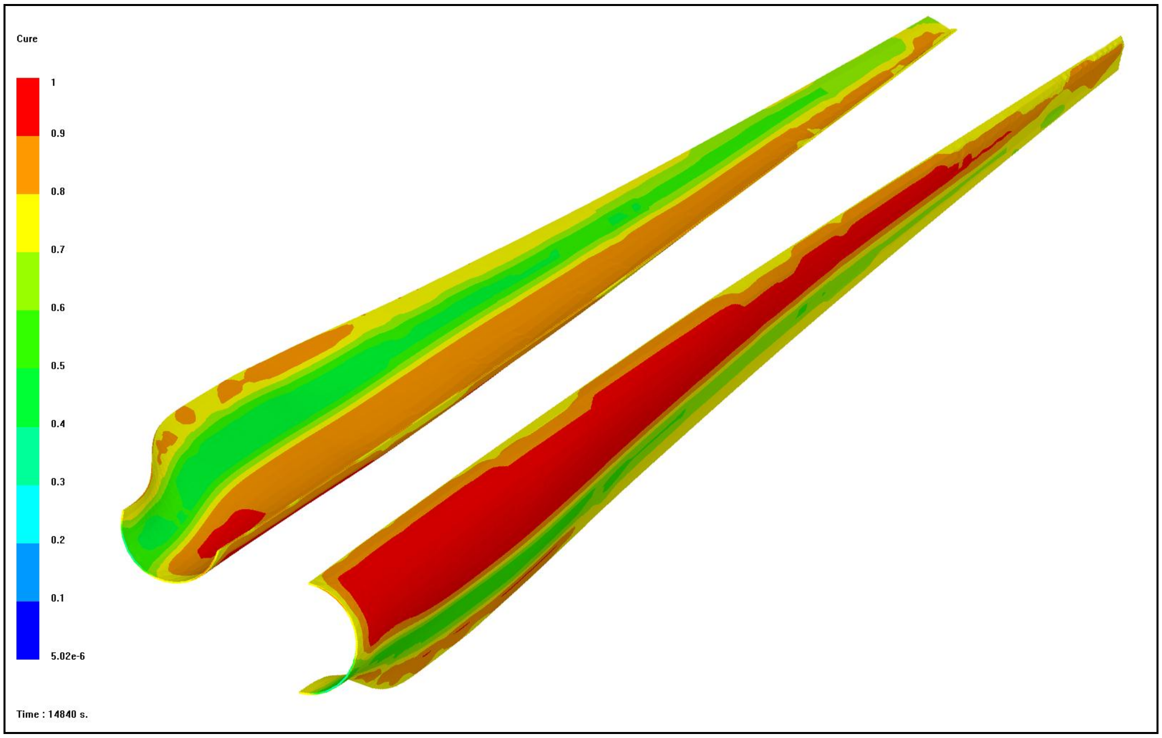

Figure 15. Degree of cure at 14,840 s.

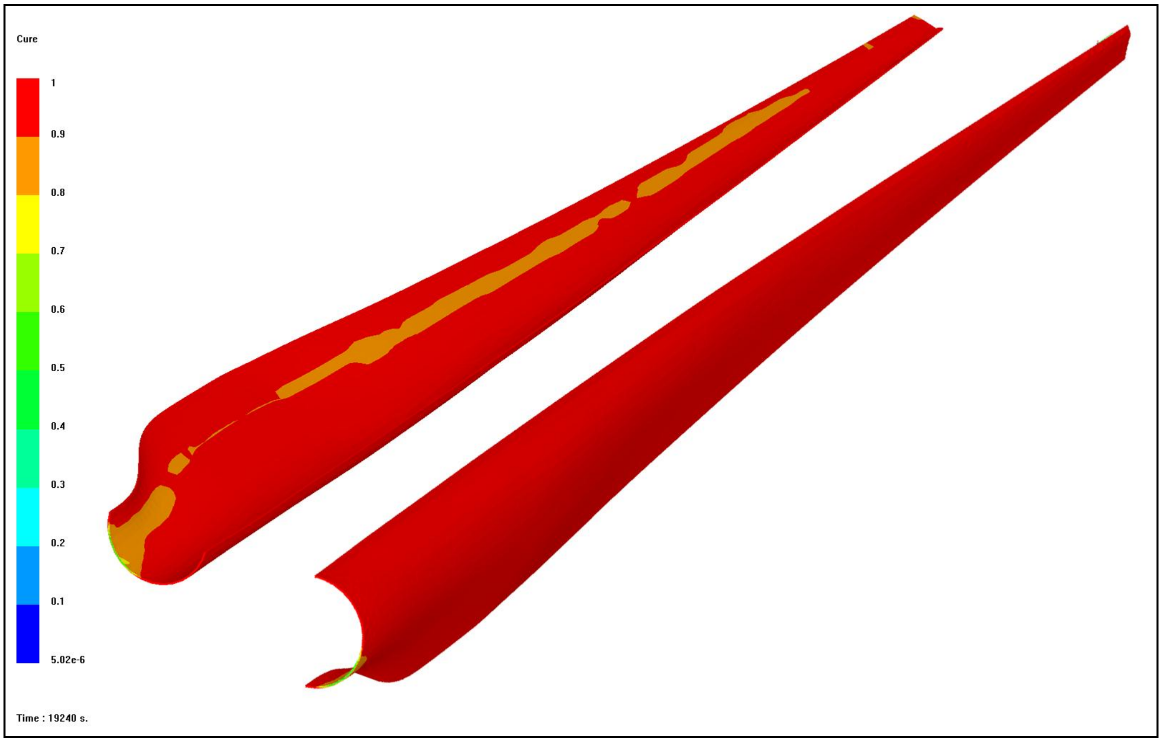

Figure 16. Degree of cure at 19,240 s.

Figure 17 shows the degree of cure at three different points through the thickness direction of the blade. The figure shows that the cure at the mold side (point C in the figure) is faster compared to the cure at the middle of the part and at the vacuum bag side. However, the final cure state is the same for all three points at the end of the cycle. This is because the heat transfer coefficient in the mold side is lower than in the vacuum side and, as a result, the temperature initially increases more at point C making the cure proceed faster at this point.

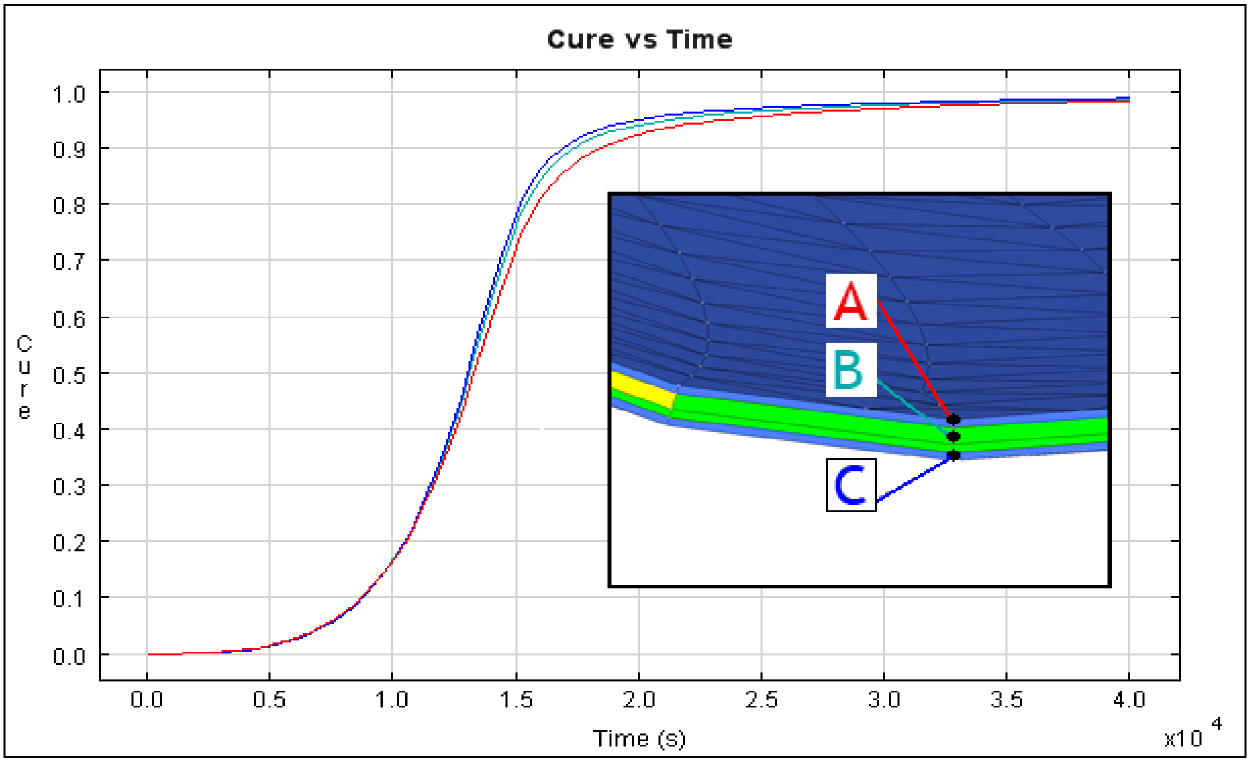

Figure 17. Degree of cure history of the part at three different points through the thickness direction of the blade.

The temperature distribution during cure after isothermal filling can be seen in Figures 18-21. From these figures, the temperature in the part (except in the core area) starts to increase significantly at approximately 10,000 s (when the cure extent reaches approximately 10%-15%) and it reaches the maximum temperature of 366 K at around 15,000 s (when the curing extent is in the range of 70%-100%). Then, as cure continues, the part starts losing heat via convection until it reaches room temperature at around 40,000 s.

Regarding the core areas, the maximum temperature reached in the core area is around 35 K lower than in the non-core areas (see Figure 21). In terms of cure extent, curing in the core area proceeds in a similar pattern than in the non-core areas except for the fact that the curing rate is significantly lower. This results in a time delay for curing of approximately 15,000 s towards the end of the curing cycle (see Figure 22). Yet, the curing extent for the core and non-core areas is approximately the same at the end of the cure cycle.

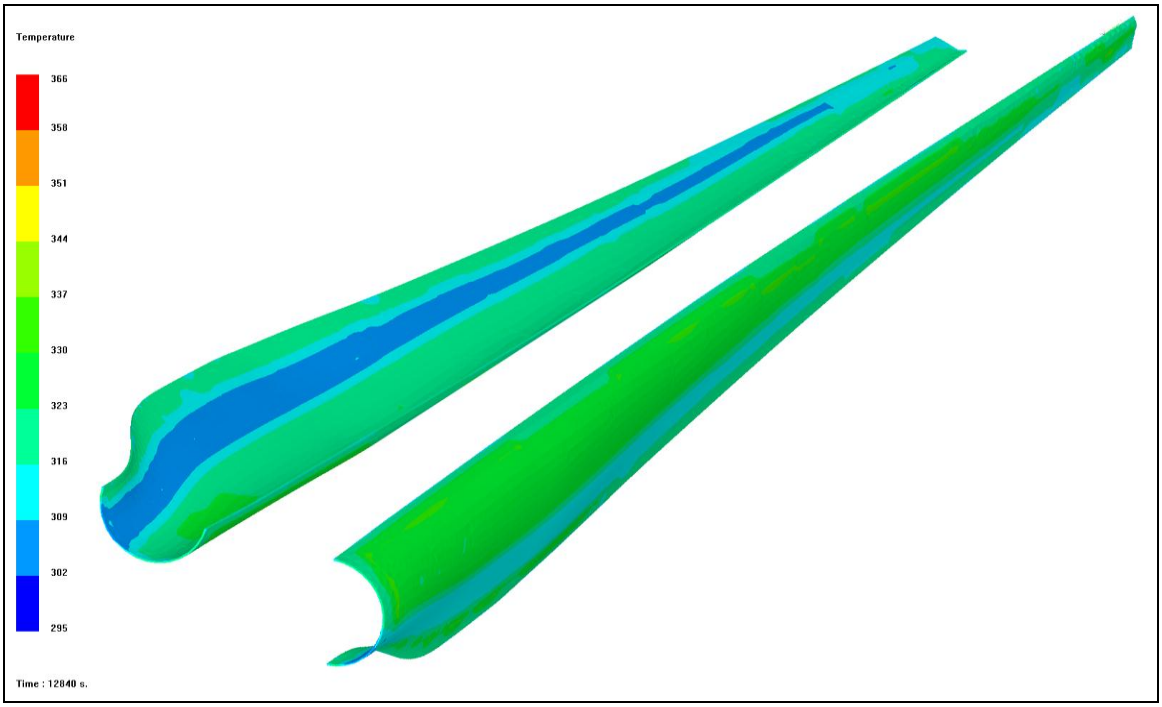

Figure 18. Temperature (K) distribution at 12,840 s.

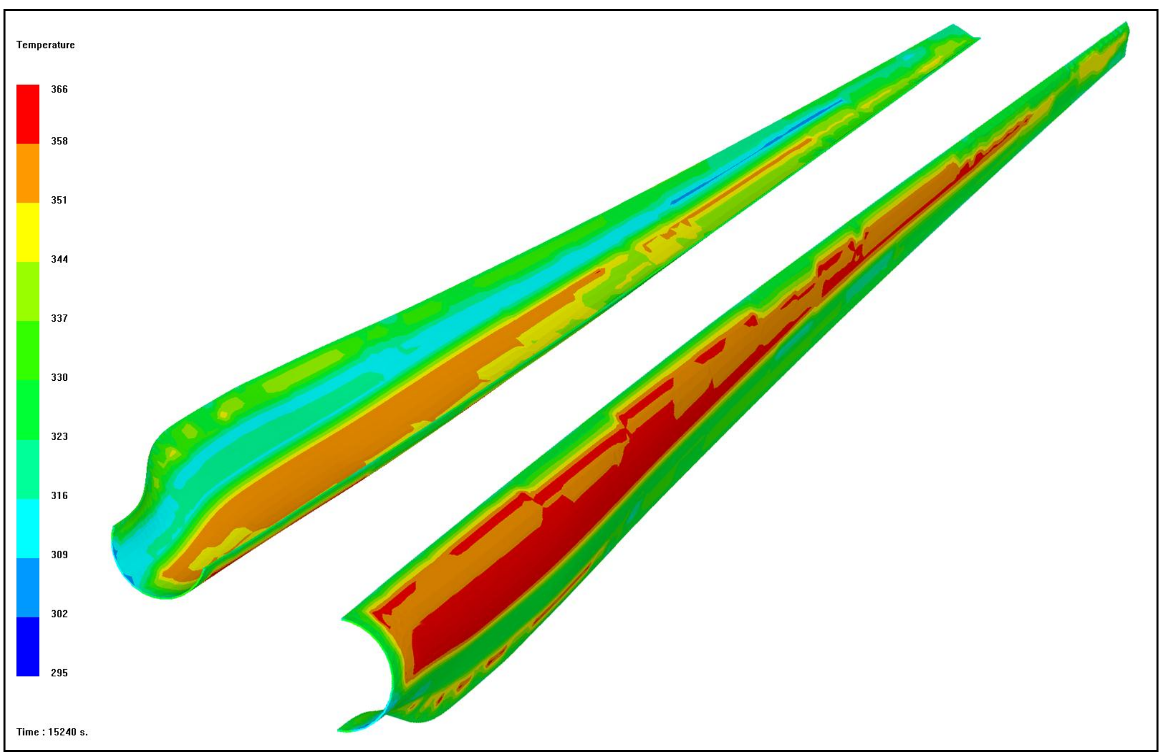

Figure 19. Temperature (K) distribution at 15,240 s.

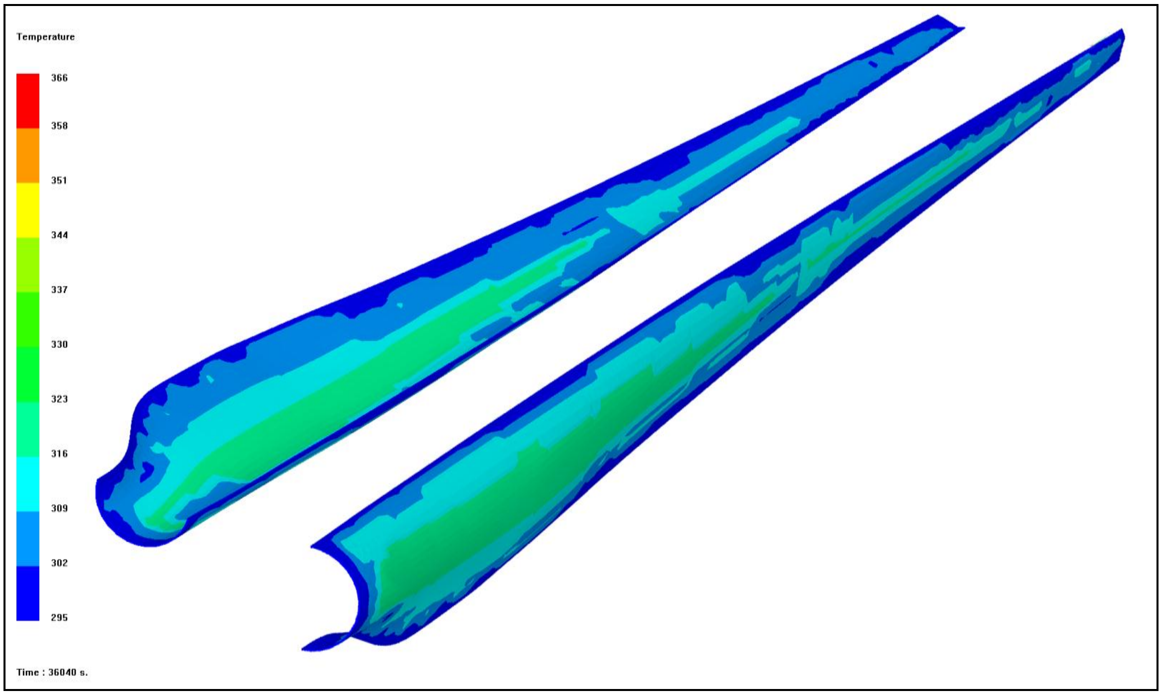

Figure 20. Temperature (K) distribution at 36,040 s.

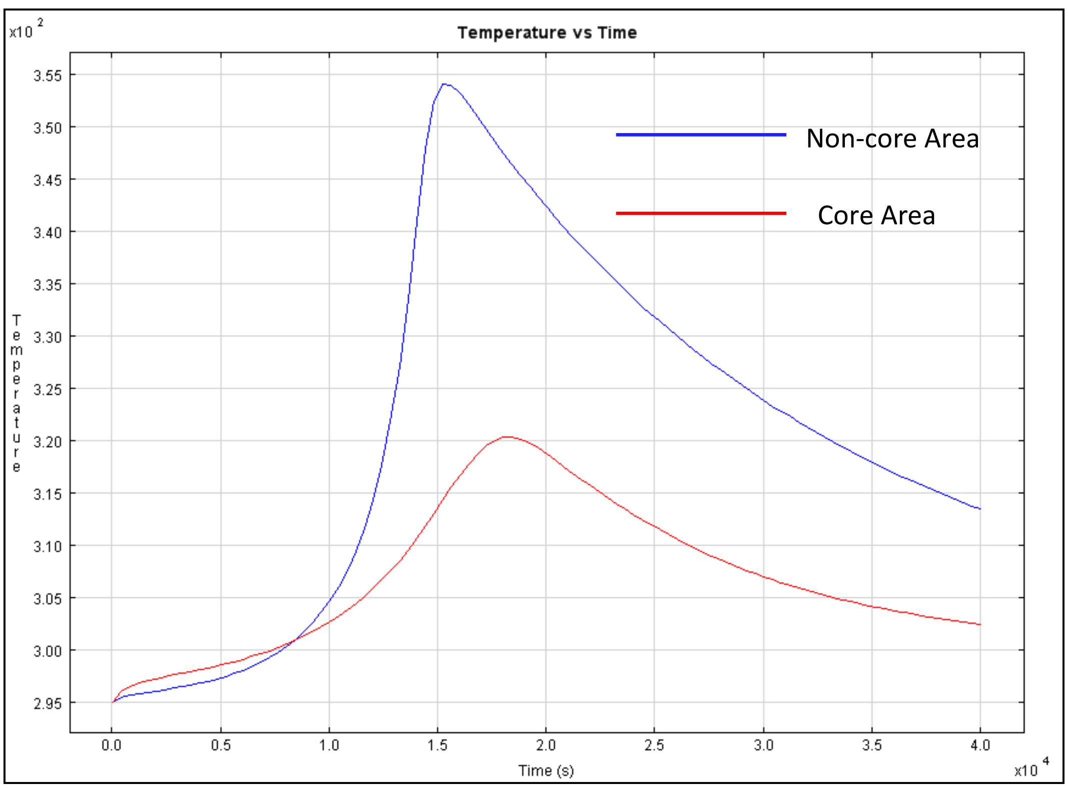

Figure 21. Temperature (K) history of core and non-core areas for the entire cure cycle.

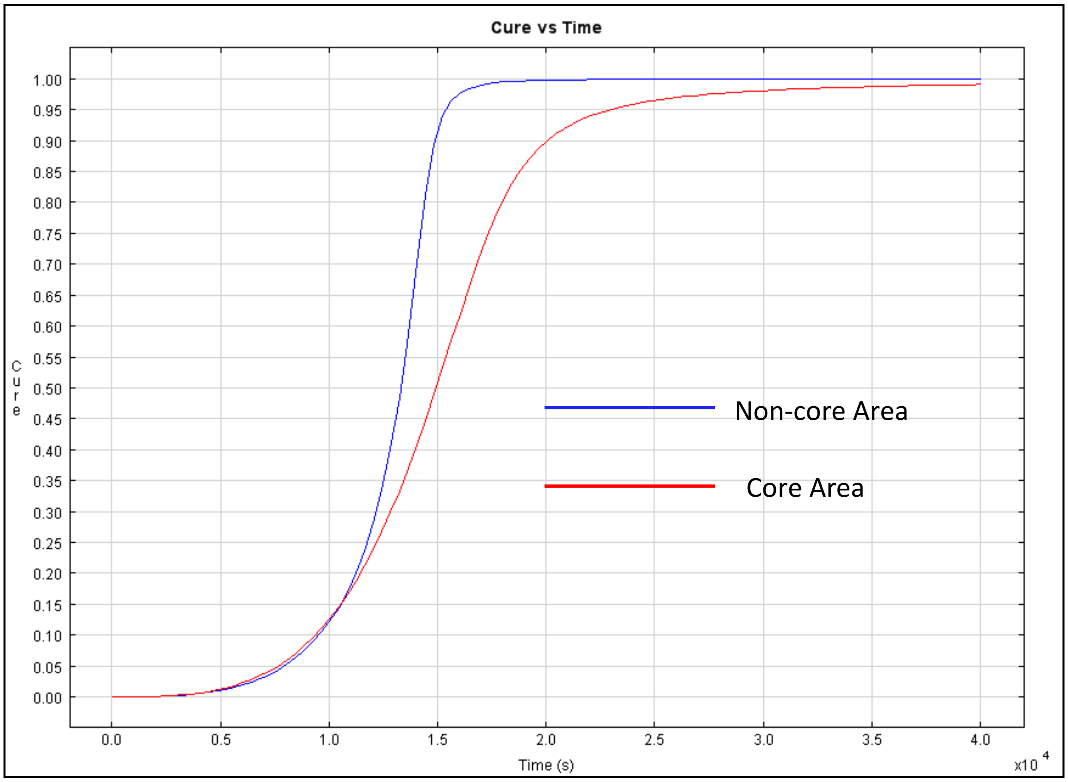

Figure 22. Degree of cure history of the part at the core and non-core areas for the entire cure cycle.

Chapter 3: 3D Non-Isothermal Filling and Curing

For this 3-D simulation, the "Mesh Extrusion" function was used to create six node pentahedral elements with respect to layer thicknesses. Figure 23 illustrates how the layers of the preform and the core material were positioned.

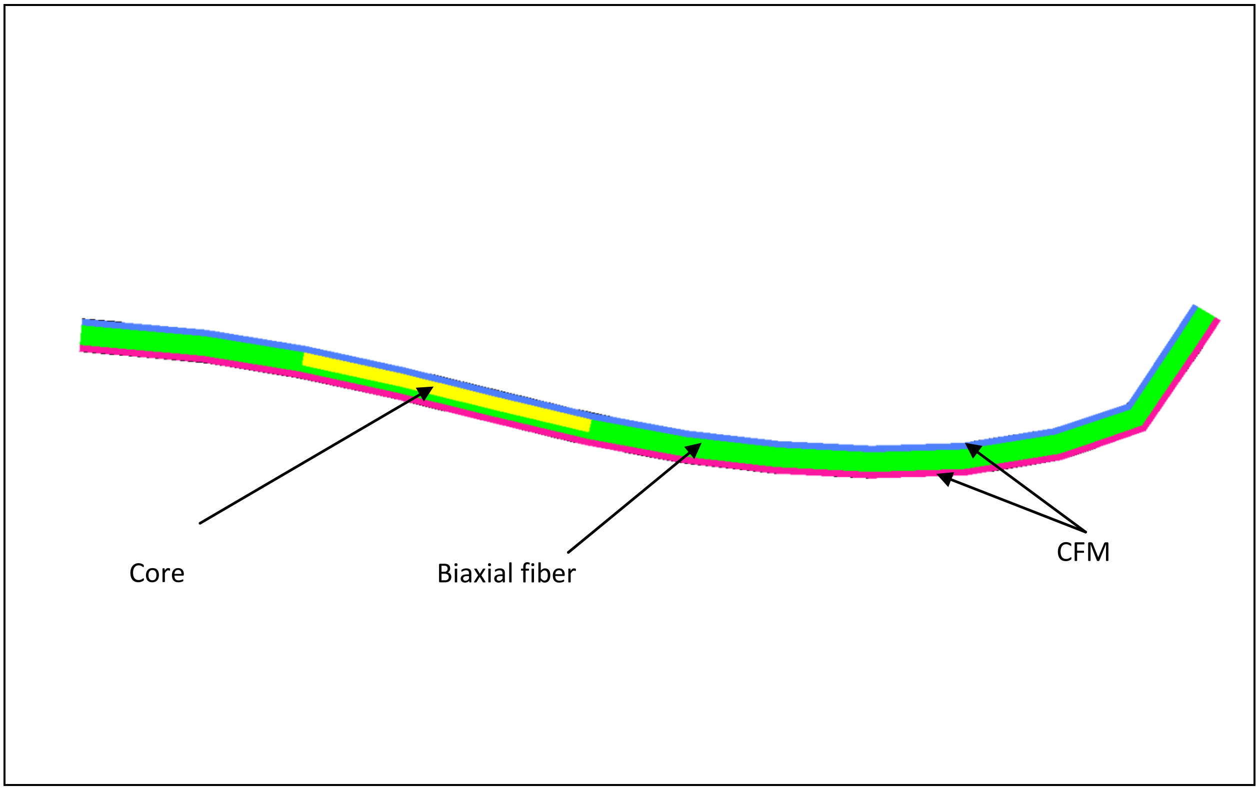

Figure 23. Cross-section of the discretized composite wind turbine blade.

Material Properties

Reinforcement and Core Material Properties

- Permeability
  - Biaxial $K_1 = K_2 = 1\times10^{-9}$ m^2, $K_3 = 1\times10^{-10}$ m^2
  - CFM $K_1 = K_2 = 1\times10^{-8}$ m^2, $K_3 = 1\times10^{-9}$ m^2
- Porosity
  - Biaxial $\varnothing$=0.5
  - CFM $\varnothing$=0.8
- Density
  - Glass fiber ρ_f = 2,565 Kg/m^3
  - Balsa ρ_c = 150 Kg/m^3
- Specific heat
  - Glass fiber C_f = 1205 J/Kg.K
  - Balsa C_c = 2900 J/Kg.K
- Thermal conductivity
  - Glass fiber k_f = 0.2 W/m.K
  - Balsa k_c = 0.06 W/m.K

The permeability orientation for all the laminates was defined as K_1 in the longitudinal direction of the blade, K_2 in the in-plane direction perpendicular to K_1, and K_3 in the through-thickness direction.

Resin Properties

The resin was assumed to be non-thixotropic and the injection process was assumed to be non-isothermal. The assumption is that the catalyst is mixed with the resin on-line before entering the part and partial curing is expected during filling. The flow behavior becomes very complex in this case since the temperature and degree of cure influence the viscosity and therefore the resin filling pattern.

For this non-isothermal filling simulation two main models were incorporated:

1. A cure kinetic model for modeling the curing and heat generation behavior of the resin.
2. A viscosity model as a function of degree of cure and temperature.

These models will be described in detail in the following subsections.

Cure Kinetic Model for Polymerization:

The model selected to simulate the curing kinetics was the Kamal-Sourour model. The Kamal-Sourour equation for a resin with *n* components is as follows:

$$\alpha = \sum_{i=1}^{n} c_i \ \alpha_i$$

$$\frac{d\alpha_i}{dt} = K_i\,(T).\alpha^{m}{}_{i}\,.(1-\alpha)^{p}{}_{i}$$

Where α is the degree of cure, C_i is the weight parameter of each reaction, K_i is the rate constant of the chemical reaction and $\frac{d\alpha_i}{dt}$ is the rate of reaction for the i^{th} component, the values of K_i are defined by the Arrhenius rate law:

$$K_i = A_i \exp\left(-\frac{E_i}{R \cdot T}\right)$$

where A_i are the pre-exponential factors, E_i are the activation energies of the chemical reaction, m_i and p_i are exponents that characterize the sensitivity of each autocatalytic reaction, R is the universal gas constant, and T is the temperature of the system.

The thermal properties of the resin used in this simulation are as follows:

- Pre-exponential factor $A = 1.8 \times 10^4\ s^{-1}$
- Activation energy $\frac{E}{R} = 5.19 \times 10^3$ K
- First exponent $m = 0.65$
- Second exponent $p = 1.35$

- Enthalpy of reaction H_r = 142000 J/Kg
- Density ρ_r = 1083 Kg/m^3
- Specific heat C = 1300 J/Kg.K
- Thermal conductivity k_r = 0.1 W/mK

Viscosity Model:

The viscosity as a function of temperature and degree of cure was modeled using the following equation:

$$\mu(T,\alpha) = B \cdot \exp\left(\frac{T_b}{T}\right) \cdot \left(\frac{\alpha_{gel}}{\alpha_{gel}-e}\right)^{c_1+c_2\cdot\alpha}$$

where

- B = $1 \cdot 10^{-7}$
- T_b = 4850
- α_{gel}= 0.4
- C_1 = 0.75
- C_2 = 0.35

Boundary conditions

Inlet Gate and Exit Vent Locations

In order to reduce the filling time, a sequential filling scheme was used. To perform sequential filling, three inlet gates were initially defined on parallel curves along the longitudinal direction of the blade: one main inlet in the center of the blade, and two auxiliary gates located half-way between the main inlet and the edges of the blade (see Figure 24). In this scheme at the beginning of the injection process, the main inlet (blue) starts injecting resin. As soon as the flow front passes the two auxiliary inlets (yellow), the two auxiliary gates are activated and they start injecting resin simultaneously until the blade has been completely filled.

The exit vents were placed on the edges of the blade that were assumed to be the locations of the last point to fill. The exit vents are shown in green color in Figure 39. The pressure at the inlet gates was assumed to be constant with a value of 1.06×10^5 MPa and the pressure at the exit vents was assumed to be zero.

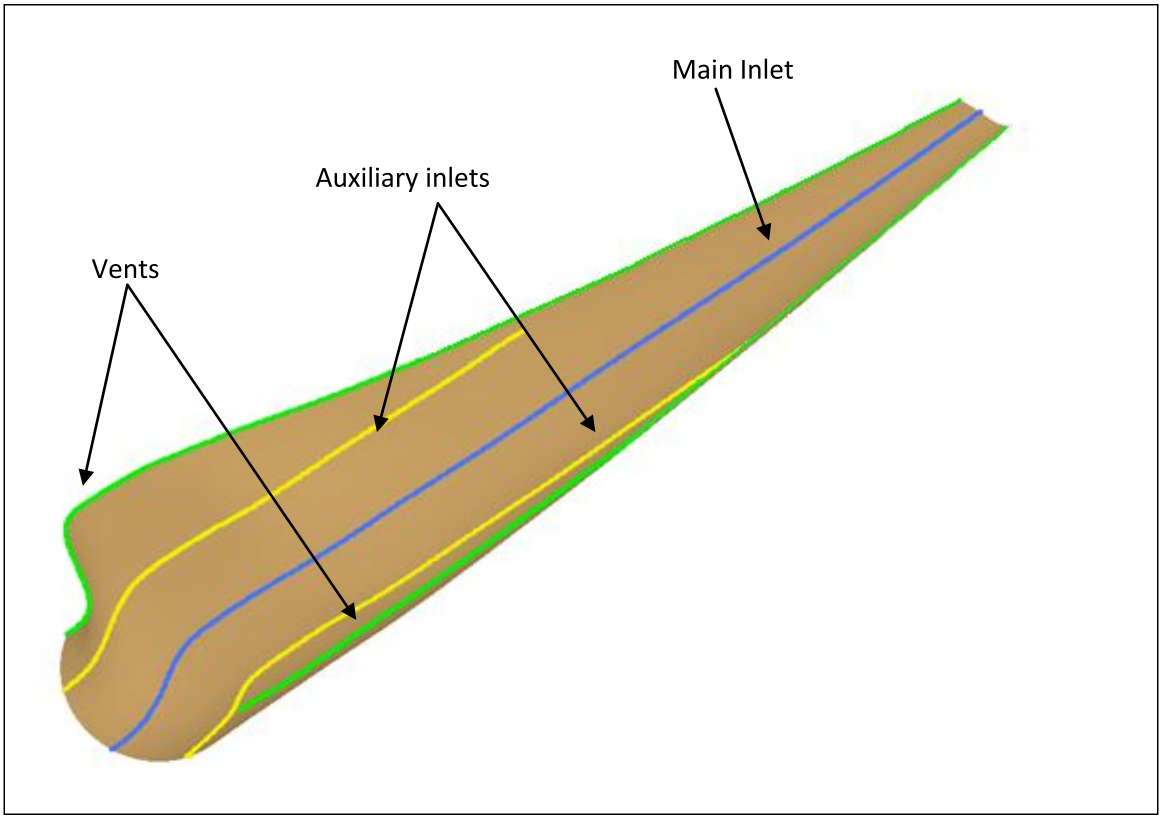

Figure 24. Location of inlet gates and exit vents.

Thermal Boundary Conditions

The resin is mixed with the curing agent online and injected to the preform at 295K. As soon as the resin is mixed with the agent, curing process begins and the generated heat from the chemical reaction is transferred by conduction through the part and also convection with the surrounding air. The areas closer to the edges and tip of the blade were assumed to have a higher convection with the surrounding air than that of the center of the blade, also the entire bottom surface (mold side) was assumed to have a constant heat transfer coefficient, as seen in Figure 25.

The mold was assumed to have no heating or cooling capabilities; the temperature of the surrounding air was assumed to be 300 K and the initial temperatures of the preform and the mold were assumed to be 310 K.

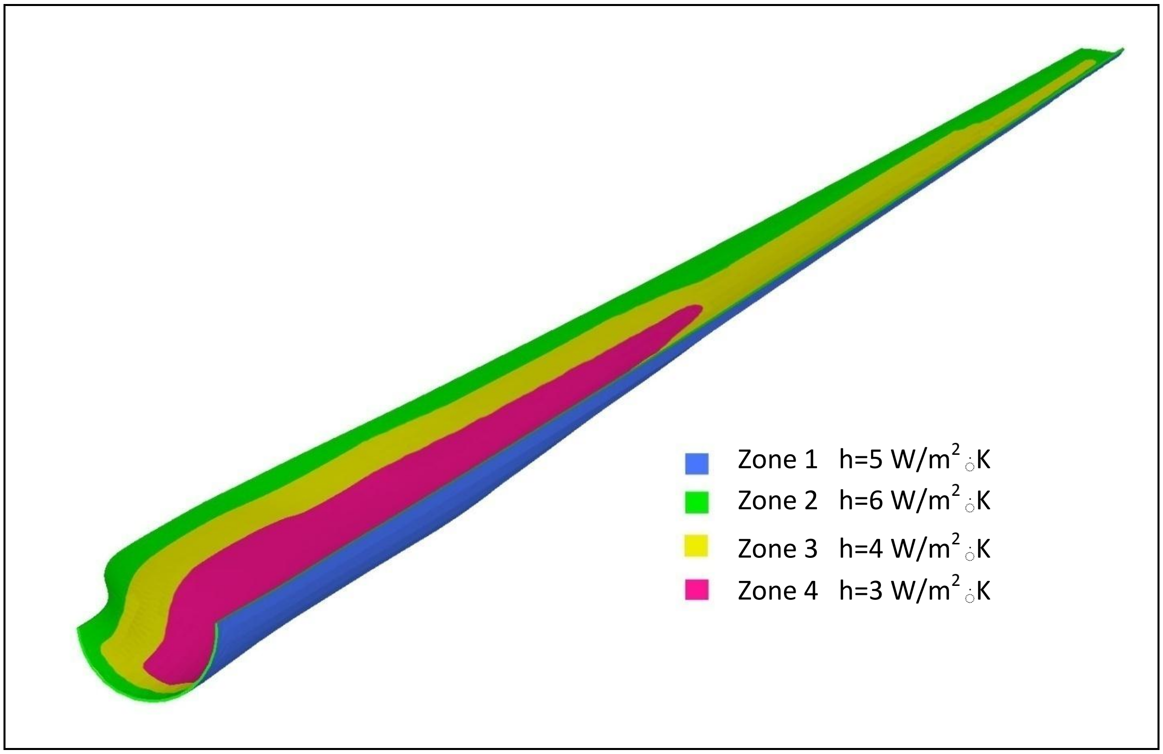

Figure 25. Heat transfer coefficient between the part and the surrounding air, and the part and the mold.

Simulations

Results for Non-Isothermal Filling Pattern

The filling pattern simulations at various times during filling are shown in Figures 26-28. At the beginning of the filling, the flow front remains nearly parallel to the inlet gate.As soon as the flow front enters the sandwich area, the velocity increases on top of the core due to the high permeability layer placed on top of the part. On the other hand, at the bottom of the part, the flow front keeps its parallel pattern through-out the filling since there is an additional 1 cm thick biaxial layer at the bottom of the core which restricts the speed of the flow (Figures 26 and 27). Figure 27 shows the filling pattern when the flow front reaches the auxiliary gates at around 1,450 seconds. At this time, the auxiliary gates are activated in order to boost the filling; and, at around 3,200 seconds the filing process is completed.

A noticeable difference in the time to complete the filling of the blade was found between the 2.5D and 3D simulations. In the 2.5D simulation the time to fill was 2,800 seconds whereas in the 3D simulation it was 3,200 seconds which represents a difference of approximately 12%. The explanation for this is as follows: (1) the mold temperature used in the 3D simulation is 10K lower than the 2.5D case which results in a higher viscosity of the resin, (2) in the 3D model, in order to avoid the formation of voids, the time to activate the auxiliary gates is governed by the layer having the least permeability which guarantees that the preform is filled up to that point before activating the auxiliary gates. In the 2.5D case, the time to activate the auxiliary gates is governed by the average permeability of the preform which in turn is higher than the lowest permeability of the 3D model, then, since the flow front in the 2.5D case reaches the auxiliary gates faster, the part is also filled faster than in the 3D case.

The last points to fill are shown in Figure 28.

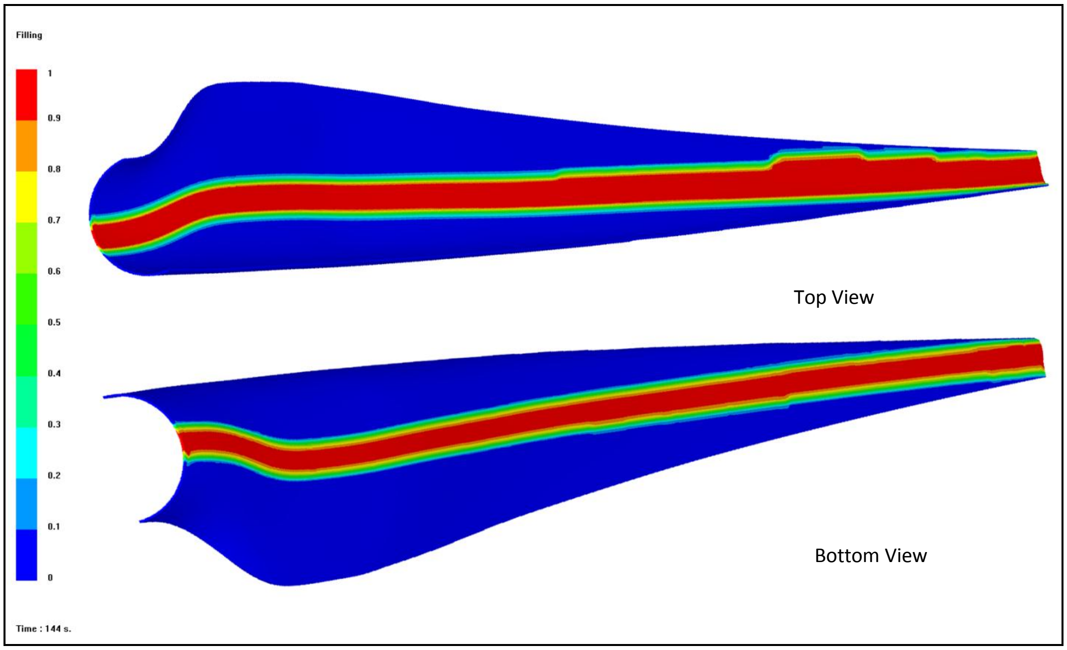

Figure 26. Filling pattern at t=144

s.

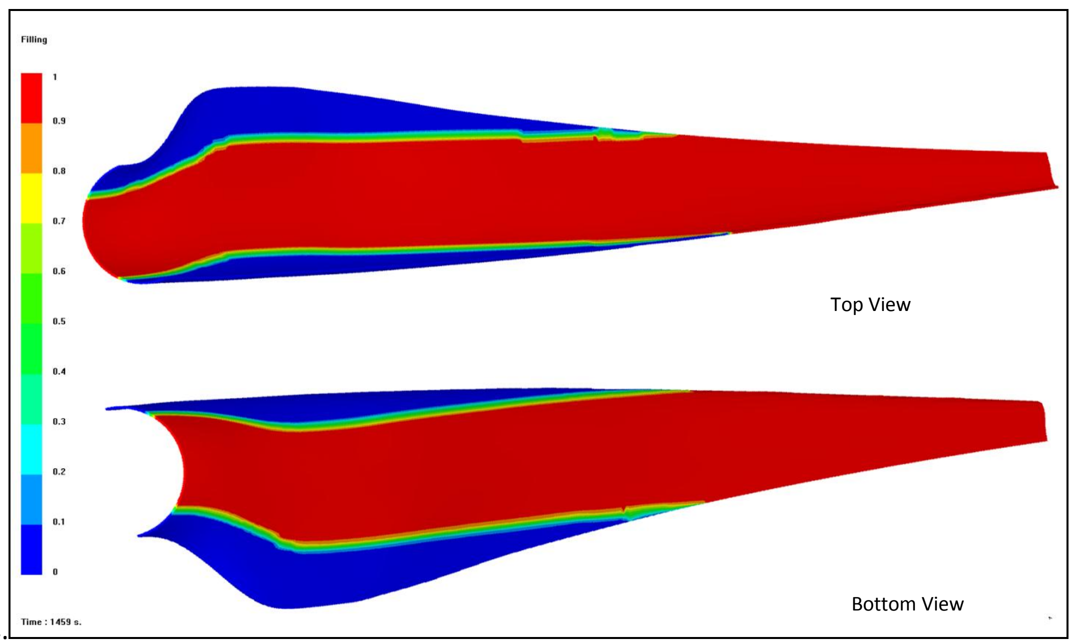

Figure 27. Filling pattern at t=1,459 s (auxiliary inlets start injection).

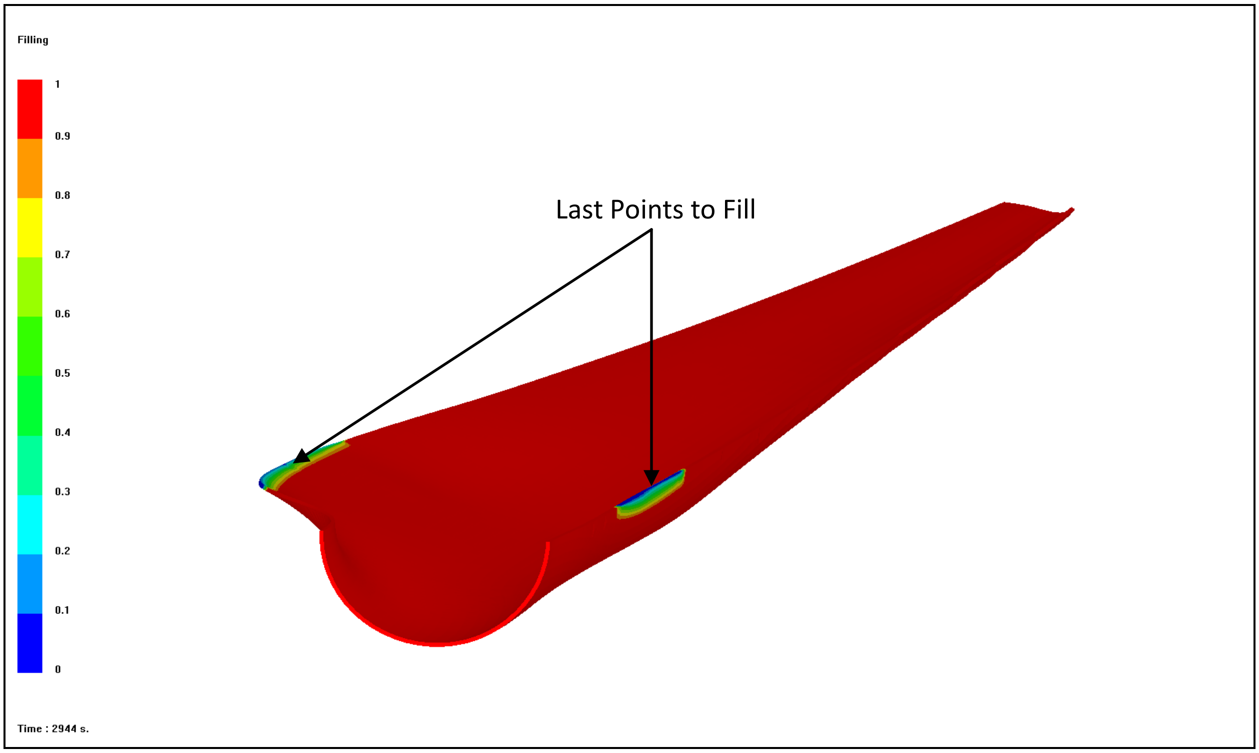

Figure 28. Last point to fill at t=2,944 s.

Results for Curing during Non-Isothermal Filling

The simulations for degree of cure during filling are shown in Figures 29-31. From Figure 29 (bottom view) it can be seen that the first areas to begin curing are where the two auxiliary inlets are located. As the filling continues, the areas adjacent to the auxiliary inlets continue curing towards the center of the blade shaping two expanding stripes that after a while converge at the middle of the part (see Figure 30 bottom view).

The activation of the auxiliary inlets explains this behavior. The activation takes place at 1,450s which eliminates the pressure gradient between the main inlet and the auxiliary gates, thus the resin injected from the main inlet stops flowing further and it stagnates in the area between the main and auxiliary gates. Since this stagnated resin was injected prior to the resin injected in other areas, it starts curing at this location before other areas. The curing of the sandwich area is wider and has a significantly higher degree of cure. This mainly takes place due to the heat transfer from the initially 15 K warmer core layer. The amount of resin is comparatively low in that area and therefore the temperature rises relatively fast and accelerates the curing.

As expected, all Figures 29-31 show higher degree of cure at the bottom of the blade. By considering the fact that the direction of the flow is through the thickness direction of the preform (top to bottom), it is apparent that the resin at the bottom was injected prior to the resin on the top and therefore starts to cure sooner.

Comparing the curing patterns in 3D and 2.5D simulations, a major difference is observed in the areas adjacent to the tip of the blade. In the 2.5D case the tip was the first point in which the aforementioned partially cured strips converged; in the 3D case however, the convergence takes place in the middle of the part prior to other areas and the tip retains its low degree of cure until the end of filling (Figures 30 and 31 bottom view). The difference between the lengths of the exit vents in the two cases accounts for this behavior. Unlike the 2.5D case, the exit vents in the current simulation were extended to the tip of the blade with the aim of eliminating some minor dry spots observed in the tryout simulation. Since the auxiliary inlets do not extend all the way to the tip of the blade, the resin injected from the main inlet in the tip region keeps flowing until the end of the filling the resin bleeding from the exit vents at the sides of the tip area guarantees having newly mixed resin in that region. Apparently this resin starts to cure after other areas start to cure.

Also, a 20% difference can be observed between the degrees of cure in the 2.5D and 3D cases at the end of filling. Figure 31 shows that the maximum value of 41.5% degree of cure has taken place exclusively in the sandwich area; in the 2.5D simulation, a maximum of 21.5% of cure extent has taken place on the sides of the part away from the sandwich area. This allows one to conclude that the 2.5D simulation was not able to take into account the heat transfer effects of the core.

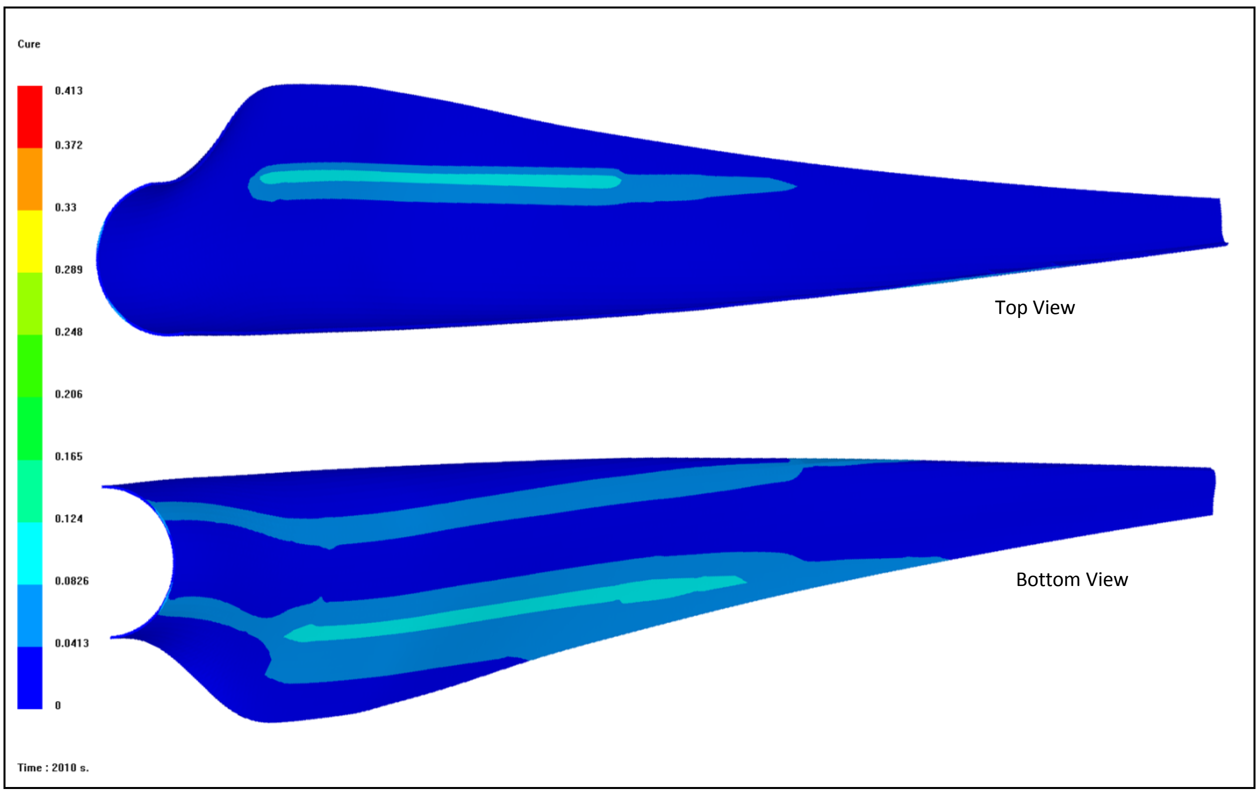

Figure 29. Degree of cure at t=2,010 s.

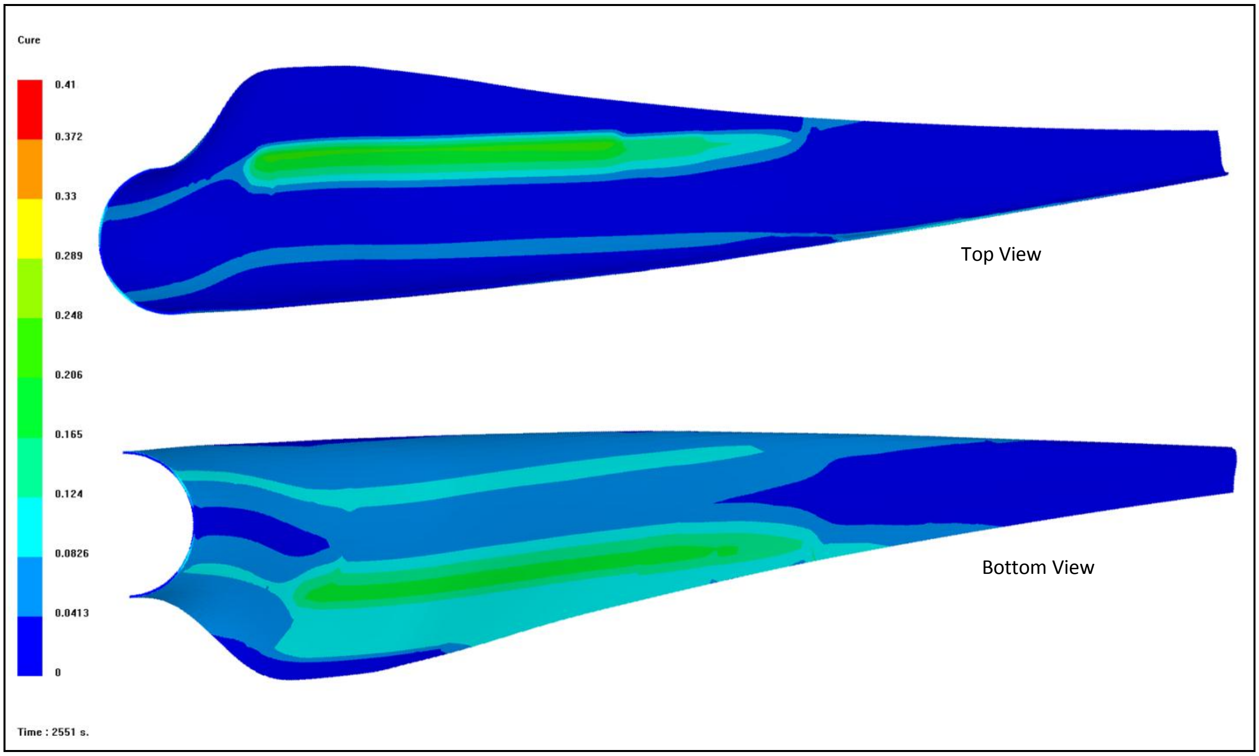

Figure 30. Degree of cure at t=2,551 s.

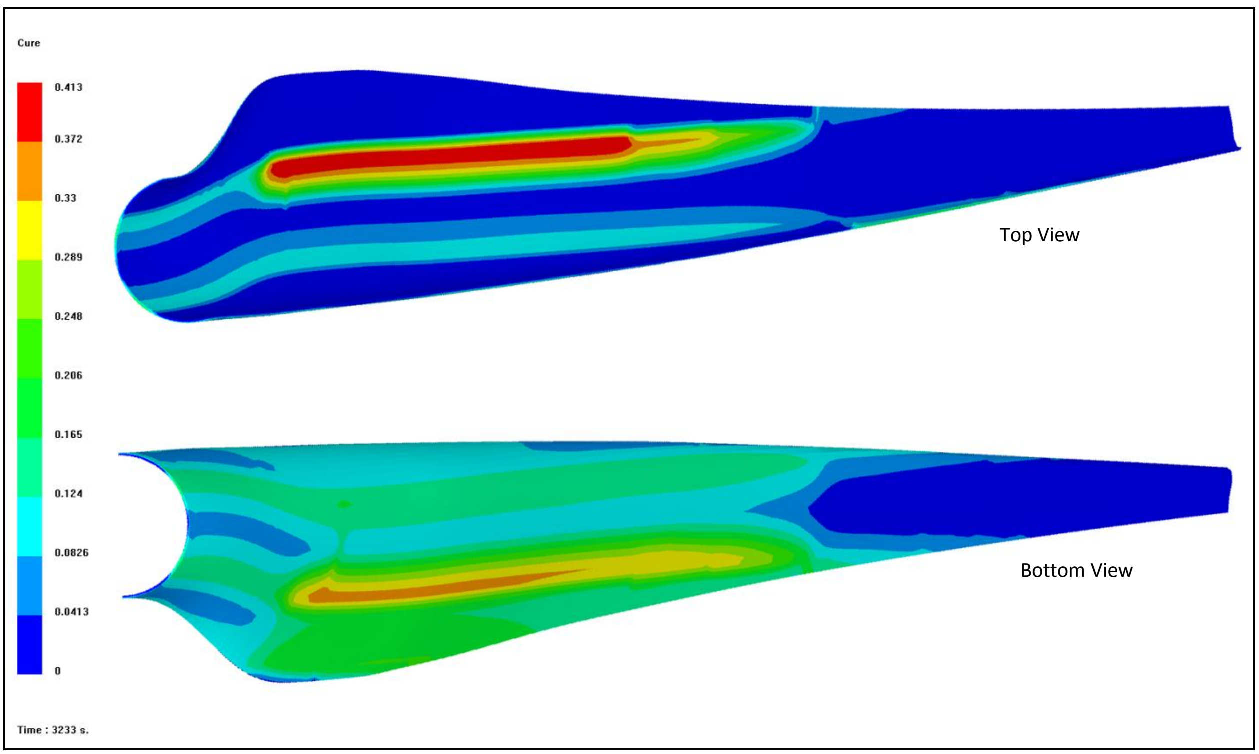

Figure 31. Degree of cure at the end of filling.

Results for Temperature Distribution during Non-Isothermal Filling

The simulations for temperature distribution during non-isothermal filling are shown in Figures 32 and 33. Figure 32 shows the temperature distribution shortly after the auxiliary gates are activated. At this time, the area between the two auxiliary gates had been totally filled. The main observation in the figure is that the area containing the core material is warmer than the remaining filled portion of the blade.

Figure 32 shows the temperature distribution at the end of filling. Similar to figure 31, the sandwich area still has the highest temperature compared to the rest of the part. The reciprocal heat transfer between the resin and the core explains the behavior. As previously mentioned, because the core has a 15K higher temperature than the resin, it makes the neighboring resin warmer and triggers an early curing at that area. The exothermal reaction starts taking place and the generated heat raises the temperature even further. It can also be seen that the areas at the sides of the blade are warmer compared to the areas closest to the inlet gates. This is due to the fact that the low temperature resin flows through the fiber decreasing the temperature of the preform. It is understandable that during the filling process, the areas closest to the inlet gates experience more resin flow through their cross section than the ones away from them.

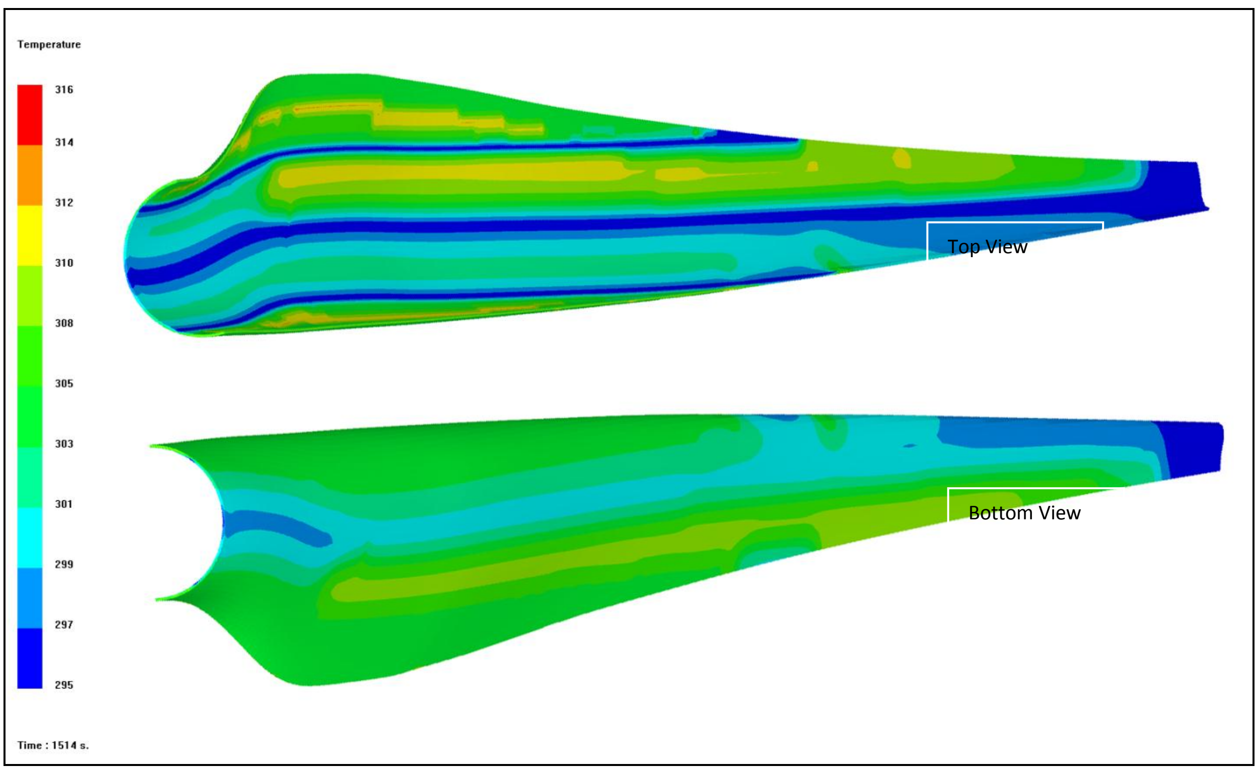

Figure 32. Temperature (K) distribution at t=1,514 s.

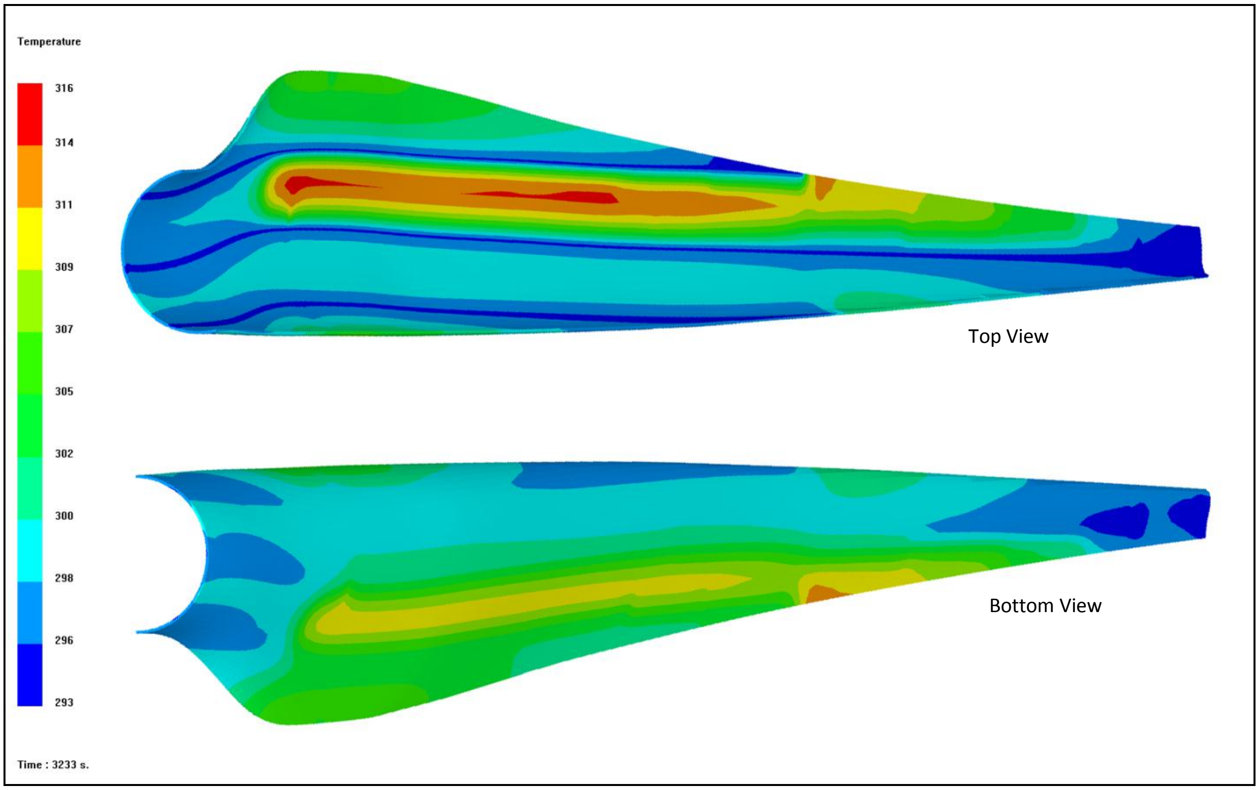

Figure 33. Temperature (K) distribution at the end of filling.

Results for Curing after Non-Isothermal Filling

The simulations for degree of cure after non-isothermal filling are shown in Figures 34-36. Figure 34 shows the degree of cure at 1,002 seconds after the end of filling. As it can be seen in the top view, the areas where the degree of cure starts after resin injection can be divided into four: two stripe-like areas located at the middle of the blade, and two areas adjacent to the edges of the blade. During cure, as time passes and curing progresses, these areas continue to cure and propagate towards the center of the blade in the transverse direction. This process continues until they finally converge and the curing is completed at around 5,000 seconds after the end of filling (see Figures 34-36). This is an expected behavior since the direction of propagation is based on the order the resin in each area was mixed and injected. The last areas to cure are those closest to the inlet gates since the resin in that area was the last to be injected.

Curing time after non-isothermal filling was compared between the 2.5D and 3D cases and a difference of 2,000 seconds was observed. If filling and curing times are considered, the total time for the 2.5D case was 9,800 seconds whereas in the 3D case it was 8,200 seconds.

This time difference is mainly caused by the difference between the heat transfer properties of the two models. In the 2.5D simulation, because of the nature of the mesh, every element (2D triangular) of the part has convective interaction with the surrounding air, whereas for the 3D case, convection was only defined for the outer face of the outer elements. As a result the 2.5D model gives away the generated heat faster and therefore it needs a longer time to finish curing.

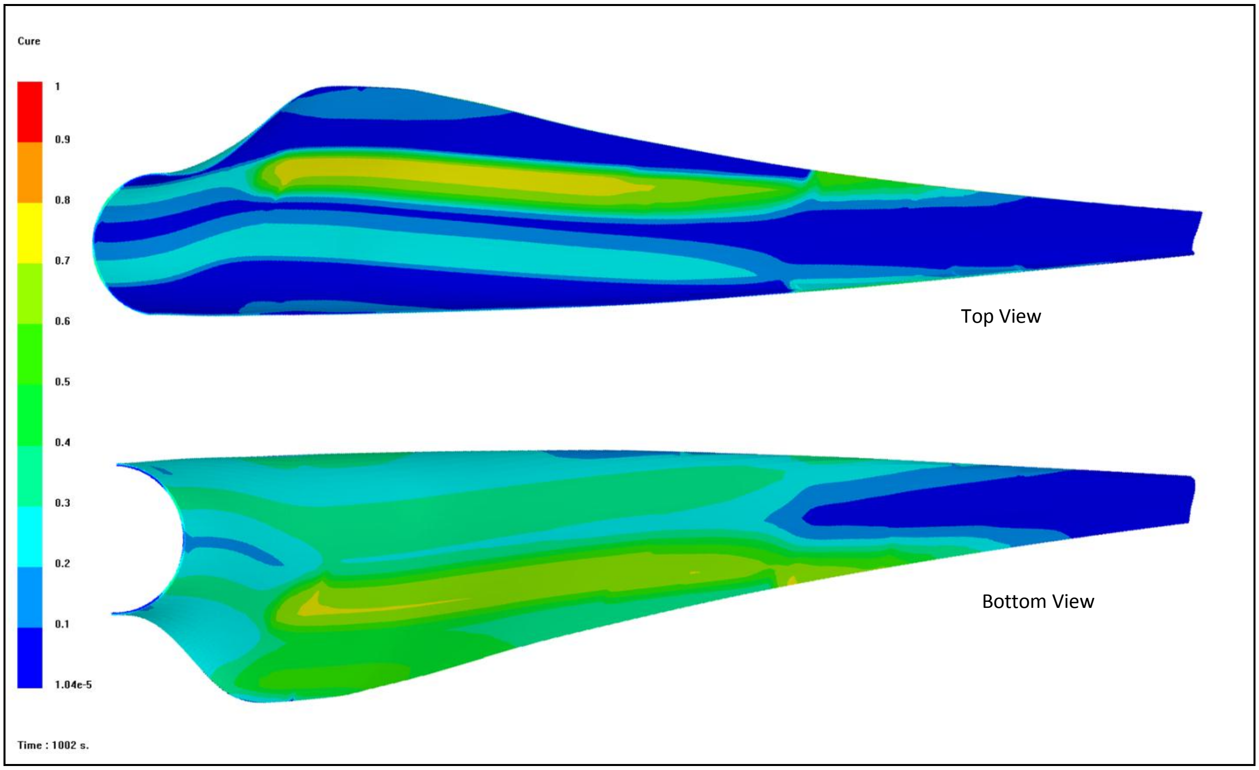

Figure 34. Degree of cure at t=1,002.

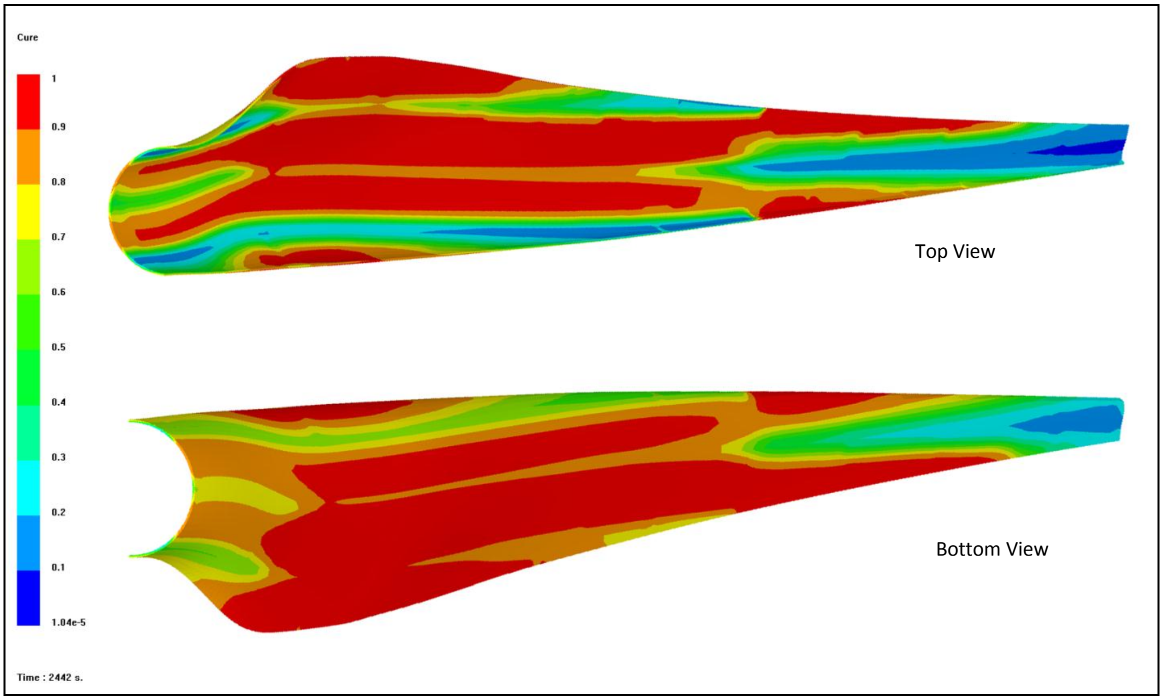

Figure 35. Degree of cure at t=2,442 s.

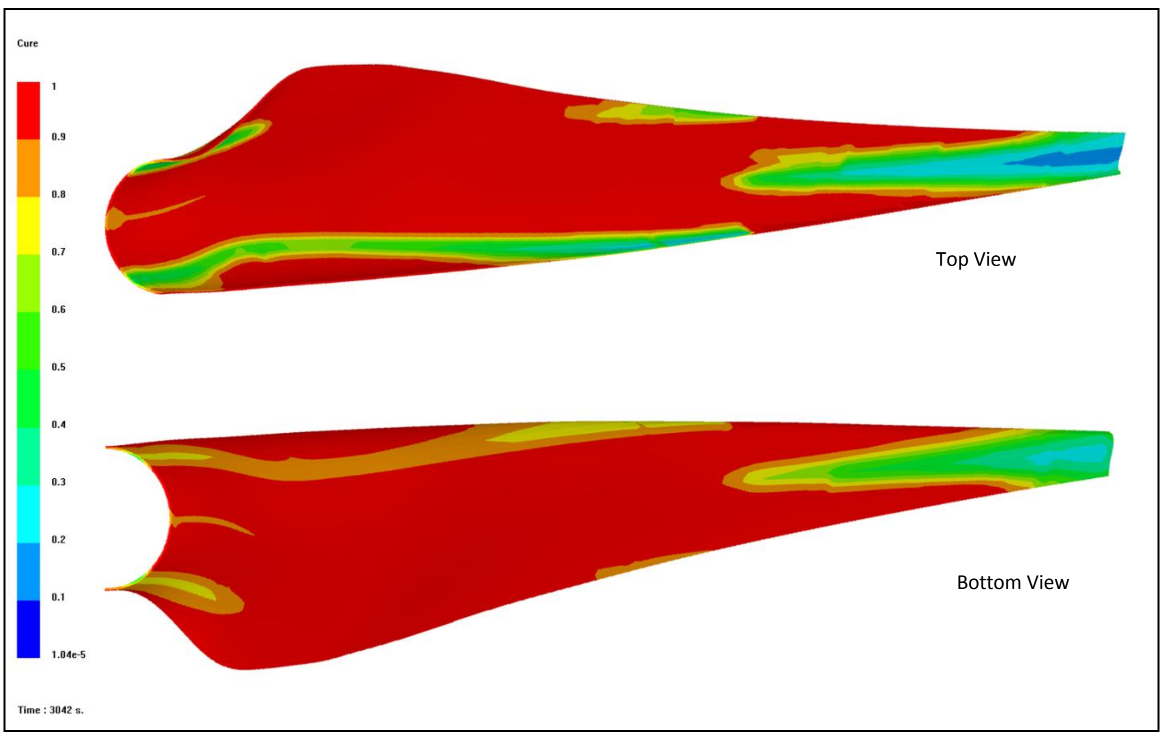

Figure 36. Degree of cure at t=3,042 s.

Temperature Distribution During Cure after Non-Isothermal Filling

Figures 37 and 38 show the temperature distribution during cure after non-isothermal filling. Figure 37 shows that the sandwich area still has a high temperature compared to the rest of the part. This is due to early curing of the resin contained on the top and the bottom of the core. Figure 38 shows the temperature distribution at 3,042 s after the end of filling when the maximum temperature of 370 K occurred in the part. The main observation in this figure is that the sandwich area is no longer the hottest region of the part. Although the sandwich area maintained a moderate temperature, the neighboring areas rose by about 40 K. The core area reached its highest temperature of 333 K at around 2,000 s after the end of filling. The explanation for this temperature difference is that the core is not permeable and therefore the laminate in that area contains much less amount of resin, hence less heat is generated during cure.

In the 2.5D simulation the part reaches the maximum temperature of 350K which is 20K lower than of the current simulation. This is in agreement with the justification that was made at the previous section for the late curing of the 2.5D case.

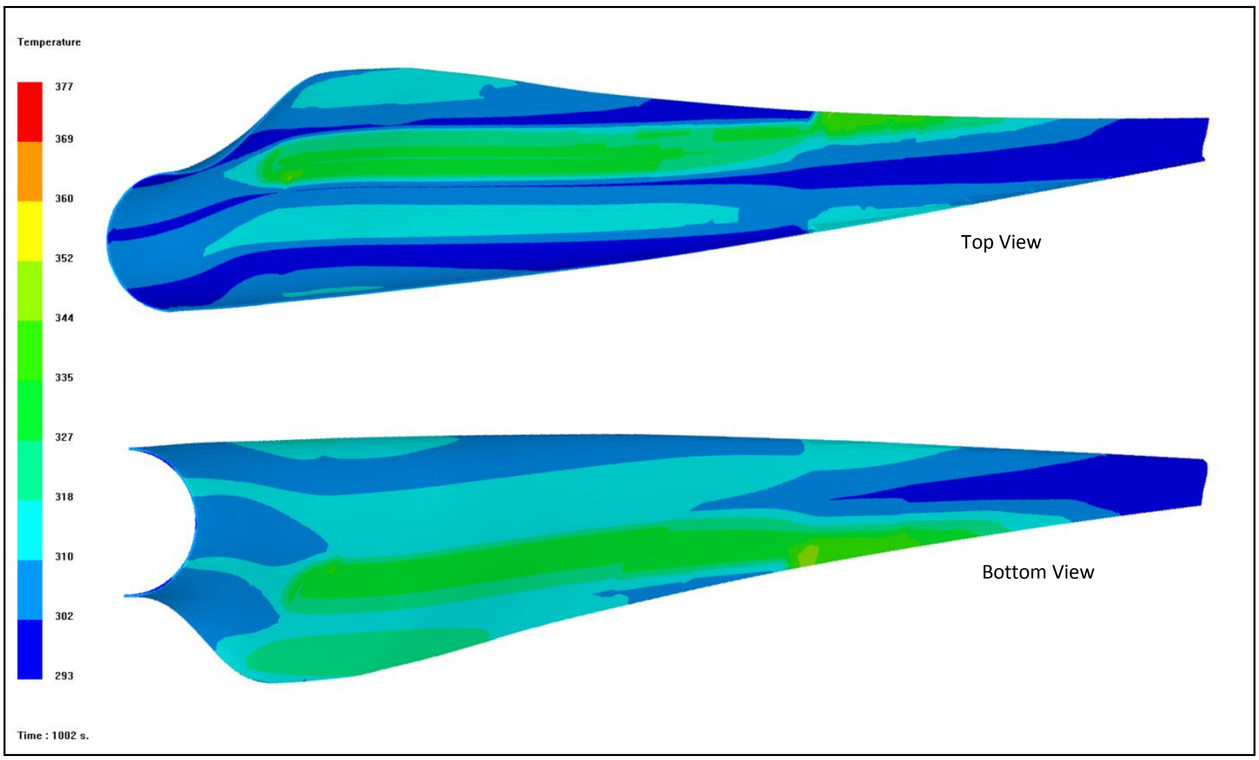

Figure 37. Temperature (K) distribution at 1,002 s.

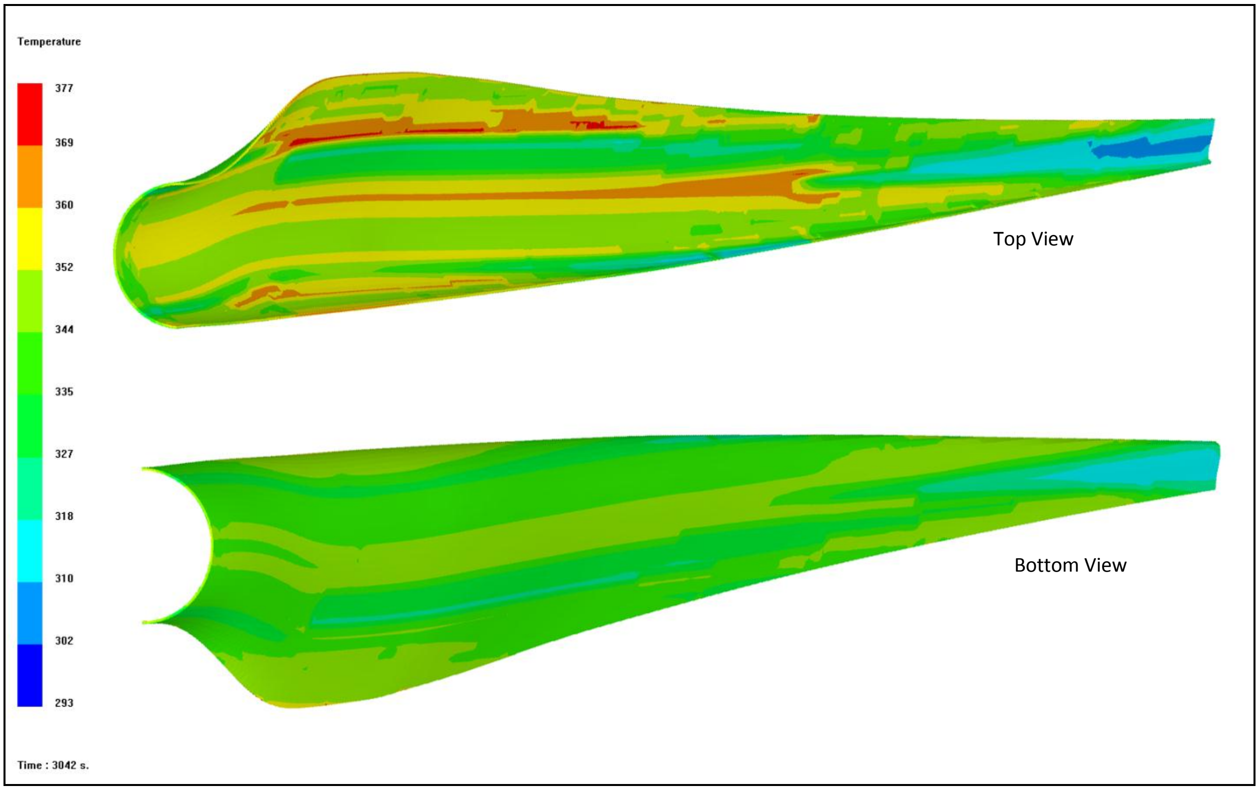

Figure 38. Temperature (K) distribution at 3,042 s.

Chapter 4: Optimization

Simulation Results

Once the model was prepared, the next step was to investigate how process variables affect the resulting process. The goal was to optimize the process by shortening the injection time. The general format of positioning inlet lines and outlet vents was taken from the format being used by the wind blade industry. The outlet vents are assumed to be placed on the side edges of the blade while the inlets are positioned longitudinally on top of the part to be used in the sequential filling scheme.

In this case study, different number of inlets in different positions were tried. For all cases, the main inlet was placed longitudinally at the center of the part while auxiliary gates were placed on the two sides of the main inlet. The number of auxiliary gates, their positions, and their activation times were varied for different cases. The outlet vents were defined on the side edges of the part in a same way for all cases. The mold was assumed to have no heating or cooling capabilities and the initial temperature of the mold, the initial temperature of the resin and the temperature of ambient air was assumed to be 330K, 320K, and 300K, respectively.

Case one: single inlet gate

For case one, no auxiliary inlets were placed and the resin was solely injected through the main inlet gate, indicated by color blue in Figure 39.

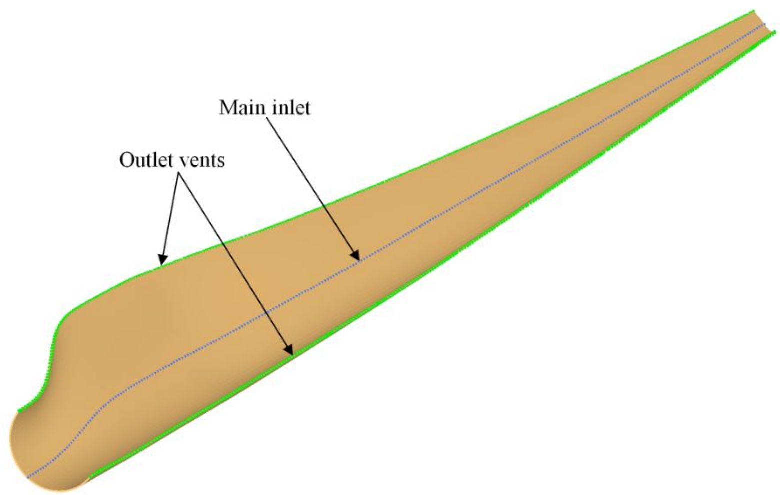

Figure 39. Inlet gate and outlet vents positioning for case 1.

For case one, the resin was not able to fully impregnate the preform and the flow stopped at 10995 seconds after the start of filling (see Figure 40). At the beginning of the filling, the flow front remains nearly parallel to the inlet gate. As soon as the flow front enters the sandwich area, the velocity increases on top of the core due to the high permeability layer and also because the core is impenetrable and there will be no flow in the through-thickness direction. On the other hand, at the bottom of the part, the flow front keeps its parallel pattern through-out the filling since there is an additional 1 cm thick biaxial layer at the bottom of the core which restricts the speed of the flow.

The resin's degree of cure at the end of filling is shown in the Figure 41. The area containing the core material started curing sooner than the remaining filled portion of the blade. The heat transfer between the resin and the core explains the behavior: because the core has a 10K higher initial temperature than the resin, it makes the neighboring resin warmer and triggers an early curing at that area.

Evidently the single inlet line failed to fully impregnate the preform due to elongation of the filling process. As can be seen in the Figure 41 the resin had reached between 40% to 100% degree of cure at the end of filling whereas the resulting high viscosity had caused total block of the flow.

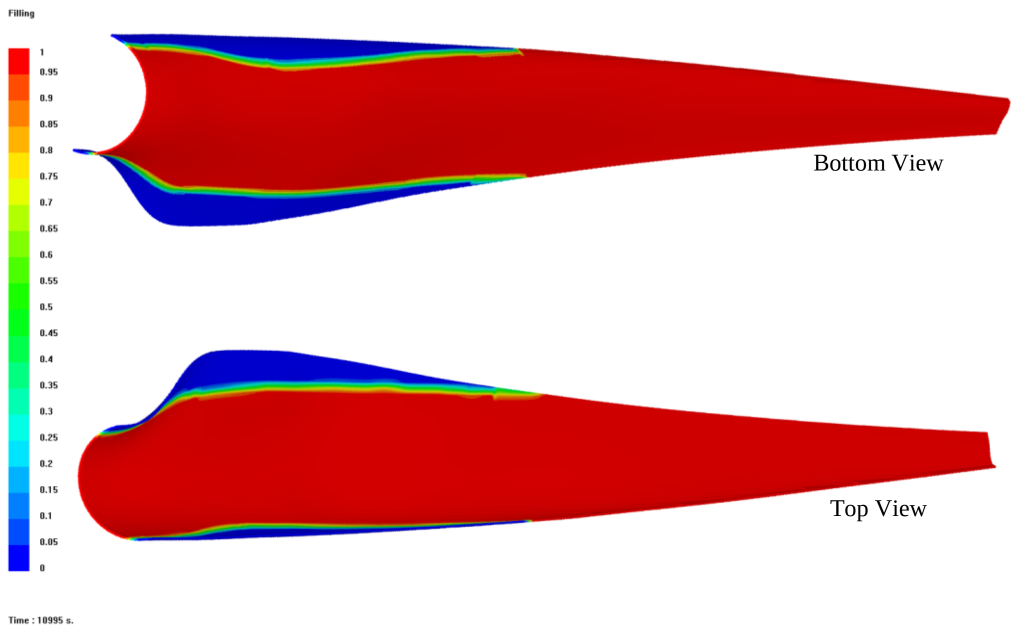

Figure 40. Filling pattern at the end of filling; t=10955s.

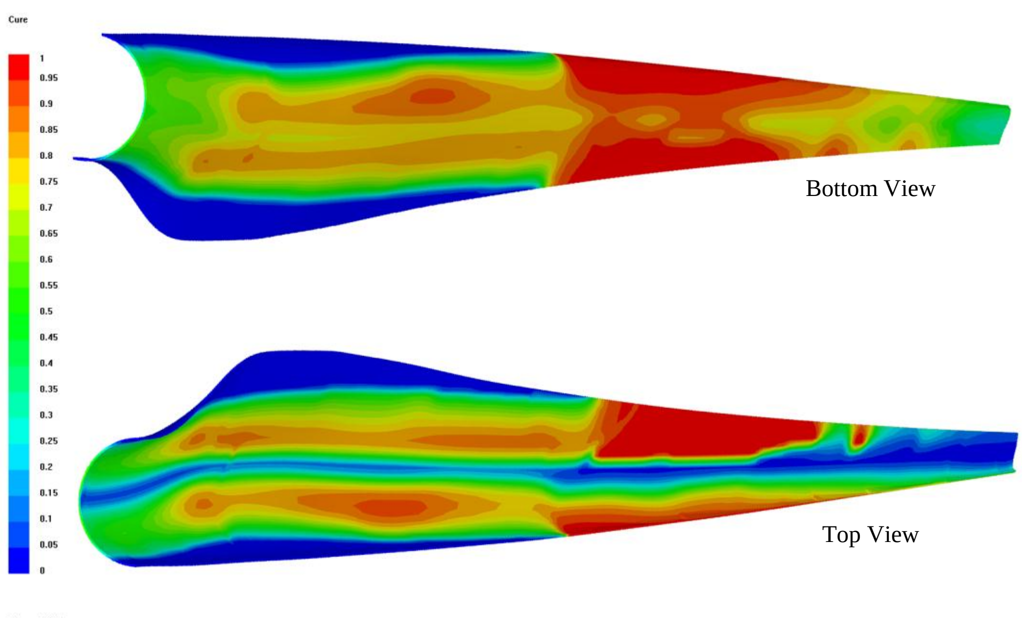

Figure 41. Degree of cure at the end of filling; t=10955s.

Case two: Three inlet gates

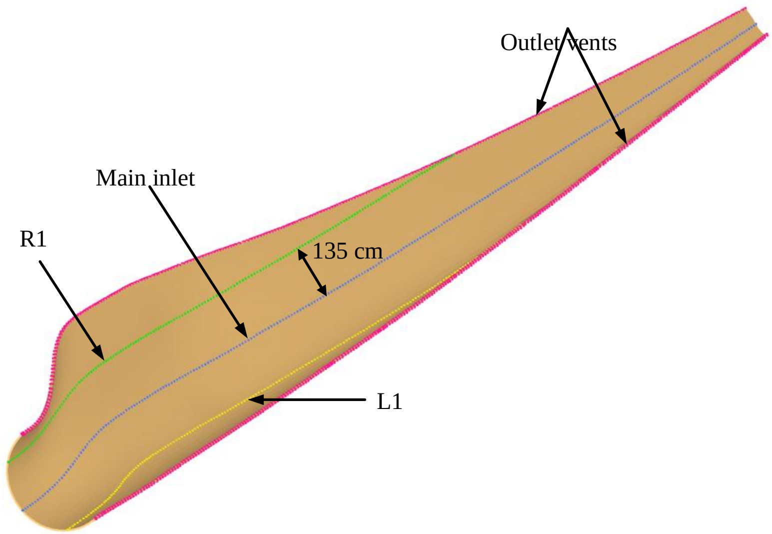

Figure 42. Inlet gate and outlet vents positioning for case 2.

For case two, one auxiliary gate was placed on each side of the main gate half way from the main gate to the outlet vents(edge of the wind blade); the inlet to the right side of the main inlet was named R1 and the inlet to the left side of the main inlet was named L1. In the first attempt, the activation time for both auxiliary gates was chosen to be 2,700 seconds after the start of filling. Figure 43 shows the part at the end of filling, in which large dry spots can be observed in the sandwich area at the bottom (mold side) of the part.

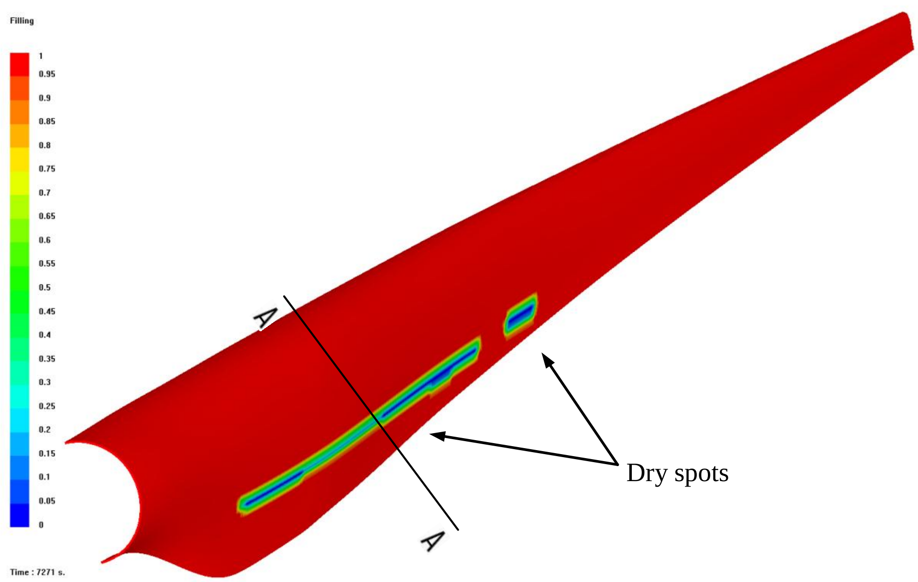

Figure 43. Bottom view of filling pattern at the end of filling.

PAM-RTM enables to show the flow pattern inside the part by sectioning it at a point of interest. In this case the part was sectioned by A-A as shown in figure 43. Figure 44 shows the structure of the part and also the location of the inlets at the section A-A.

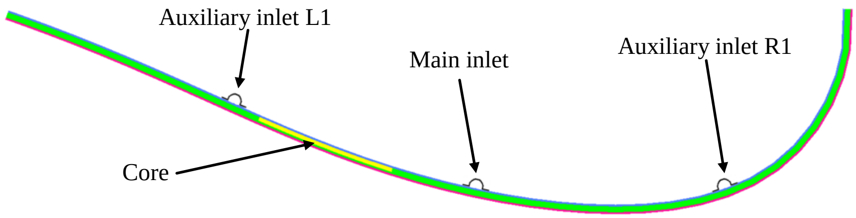

Figure 44. Core material and inlet positions at section A-A.

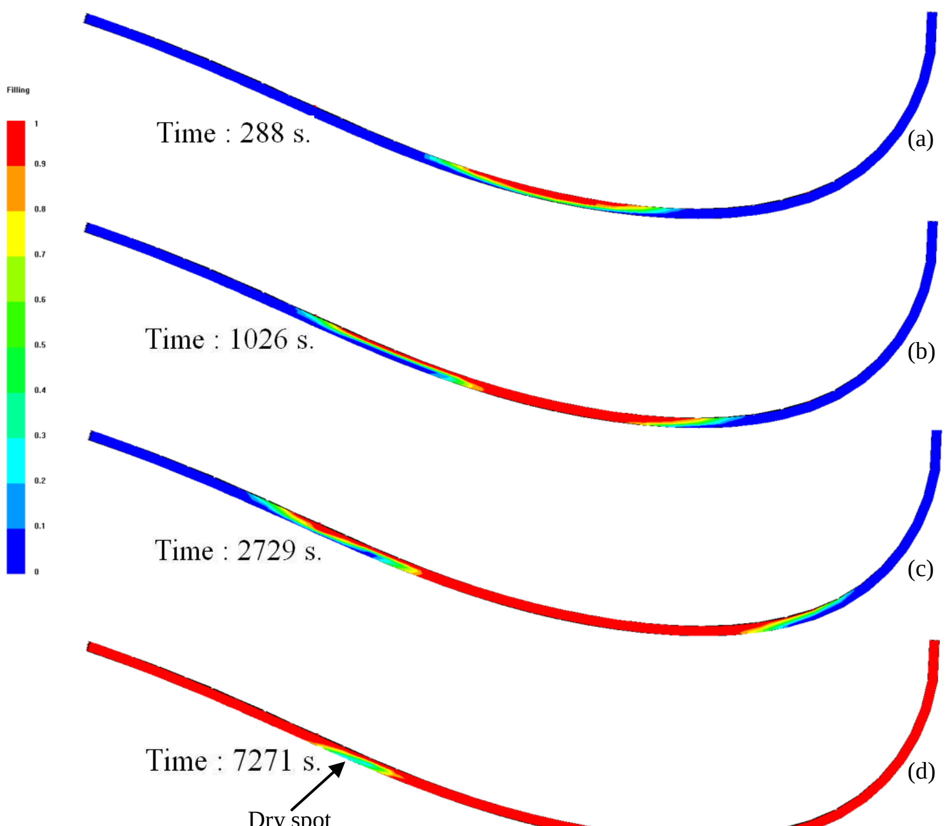

Figure 45. Flow pattern at section A-A .

As it can be seen in the Figure 45(a), the resin flows faster in the in-plane direction compared to the flow in thickness direction because the in-plane permeability values of all layers are greater than the through-thickness permeability value. As the flow front reaches the sandwich area (in the right side of the main inlet gate), it gets separated by the core material. Since the core layer is not permeable, there is no flow in the through-thickness direction in the sandwich area, and the resin flows separately in the layers on the top and bottom of the core material. The upper flow front which is already ahead of the lower flow front, gets boosted by activation of the auxiliary inlet L1 at 2,700 second after start of filling. As soon as the upper flow front passes the core, it starts infiltrating downwards in the thickness direction. Before the lower flow front can reach its way out of the sandwich area, the resin from the upper flow front reaches the bottom and blocks the way. This results in dry spot formation beneath the core.

Apparently the activation of L1 auxiliary inlet at 2,700 seconds pushed the upper flow front early and caused the formation of dry spots. Therefore a delayed activation may provide enough time for the lower flow front to leave the sandwich area on time and converge to the upper flow front without leaving voids. After several trials the activation time of 3,400 seconds for L1 resulted in full impregnation of the preform in the shortest time.

Table 1 shows the filling time and also the activation times for each of the auxiliary gates. The filling times were calculated separately for the two sides of the main inlet gate. After the activation of the main inlet gate the flow front moves to left and right direction of the main inlet in an independent way. Due to the differences in structure and the required activation times on the two sides, the filling times are different. In some cases with several auxiliary gates, the filling process in one side may end significantly sooner than the other side. Since the goal is to shorten the overall filling duration, the early impregnation in one side would be pointless, therefore a number of unnecessary auxiliary gates can be removed from that side.

Table 1. Activation times and filling duration for case 2.

Inlets	R1	L1	Left side Filling time	Right side Filling time
Activation times [s]	2,700	3,400	7,583 s	8,642 s

Case three: Five inlet gates

For case three, two auxiliary gates were placed on each side of the main gate with distance of 95 cm from each other; the location of the inlet gates are shown in Figure 46.

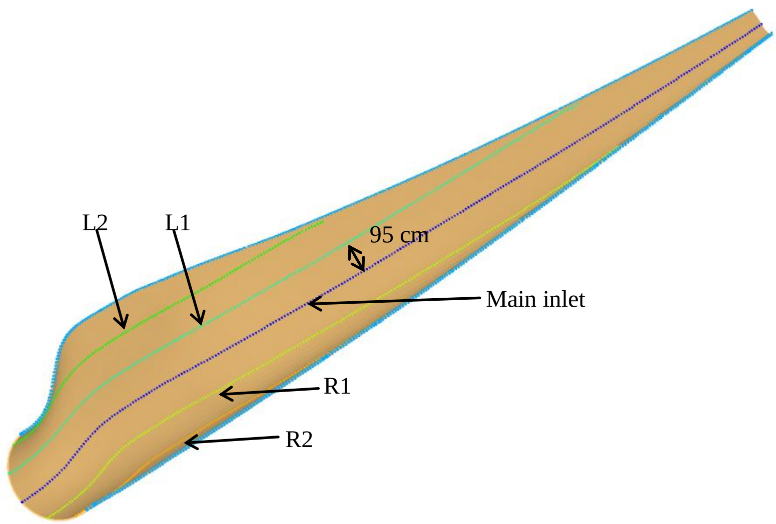

Figure 46. Inlet gate and outlet vents positioning for case 3.

The same problem discussed for the case 2 occurred in case 3. Although for the right side of the main inlet the optimum activation of the auxiliary gates managed to fill the preform in 4,947 seconds, for the left side the complications with the sandwich structure required delayed activations for the auxiliary gates. Table 2 shows the gate activation times and filling times for case 3.

Table 2 Activation times and filling times for case 3.

Inlets	L1	L2	R1	R2	Left side Filling time	Right side Filling time
Activation times [s]	2,200	3,700	1,050	2,150	5,716 s	3,902 s

Case four: seven inlet gates

For the case four, three auxiliary inlet gates were placed on each side of the main inlet gate. Figure 47 shows the location of the inlets; the distances between the inlets were tried to be kept consistent but the limitation with the mesh did not allow it, so the third auxiliary inlet on each side was placed half way from the second auxiliary gate to the outlet vent in the widest part of the blade.

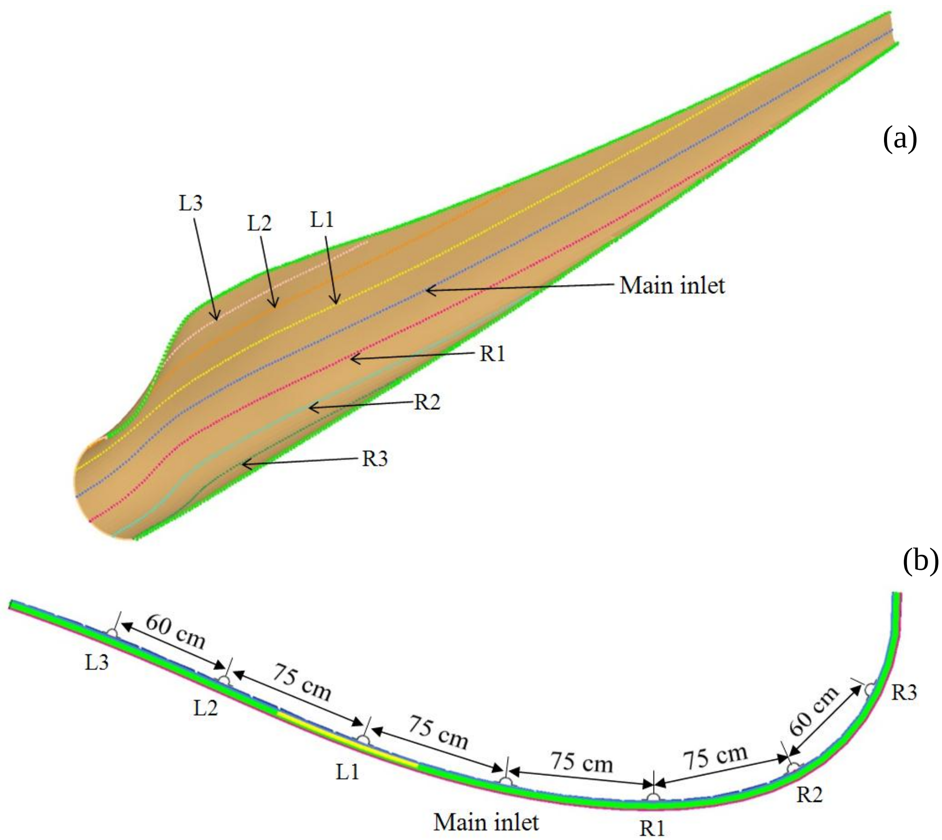

Figure 47. (a)Top view of Inlet gates and outlet vents positioning for case 4. (b)Cross section view of the inlet locations.

Different activation times were tried for the auxiliary gates and the times used in this case ate shown in Table 3 based on the shortest filling for each side.

Table 3. Activation times and filling times for case 4.

Inlets	L1	L2	L3	R1	R2	R3	Filling time (Left)	Filling time (Right)
Activation times [s]	1,800	3,200	3,600	650	1,350	1,750	4,614 s	2,571 s

Table 3 shows a significant difference between the filling times for the two sides of the main inlet gate. By looking at Table 2, it reveals that for the right side of the main inlet gate, using only two auxiliary inlets enables a complete filling in 3,902 seconds on that side, which is still less than the 4,614 seconds for the left side. Therefore using three inlets in the right side is considered an over design and using two auxiliary inlets results the same overall filling time.

Case five: nine inlet gates

Four auxiliary inlet gates were defined on each side of the main inlet gate; their locations are shown in Figure 48. Different activation times for auxiliary gates were tried; the shortest resulting filling time was obtained by the activation times shown in Table 4.

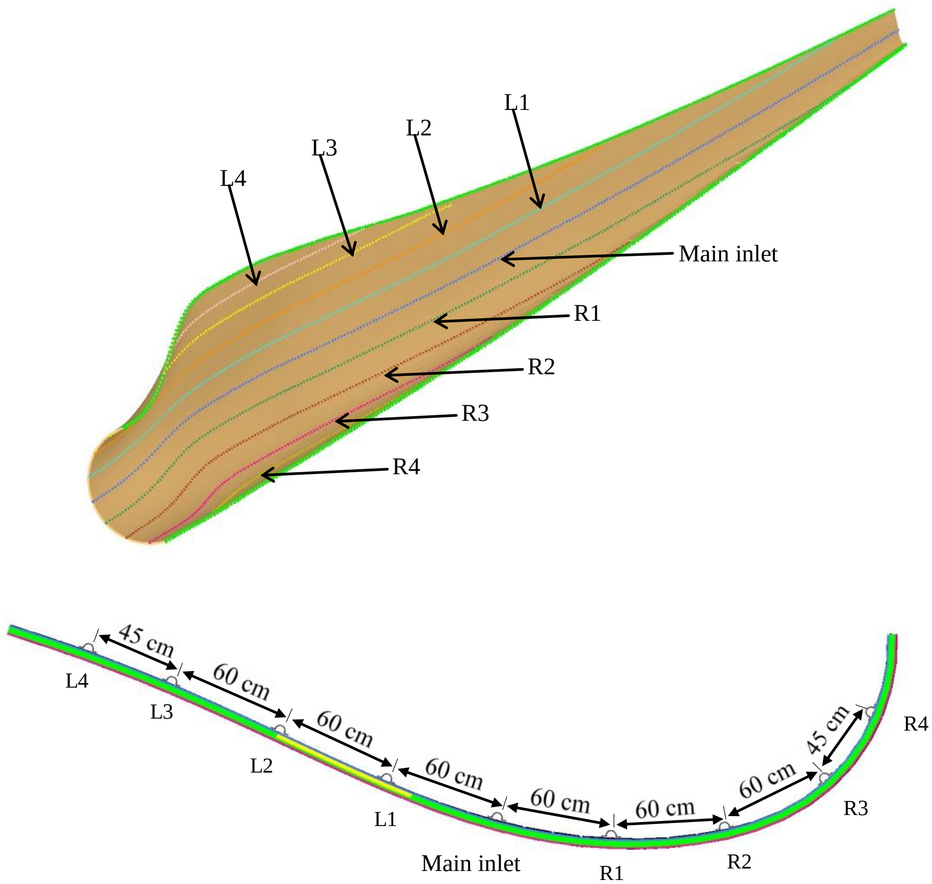

Figure 48. (a)Top view of Inlet gates and outlet vents positioning for case 5. (b)Cross section view of the inlet locations.

Table 4. Activation times and filling times for case 4.

Inlets	L1	L2	L3	L4	R1	R2	R3	R4	Filling time (Left)	Filling time (Right)
Activation times [s]	1,600	2,600	2,800	3,000	350	700	1,150	1,450	3,756 s	1,990 s

The filling time in the right side of the main inlet is significantly shorter than the left side and therefore removing unnecessary number of inlets on that side must be considered. As shown in Table 3, using three inlet gates on the right side results in a filling time of 2,571 seconds for that side, which is still less than 3,756 second for the left side.

Case six: eleven inlet gates

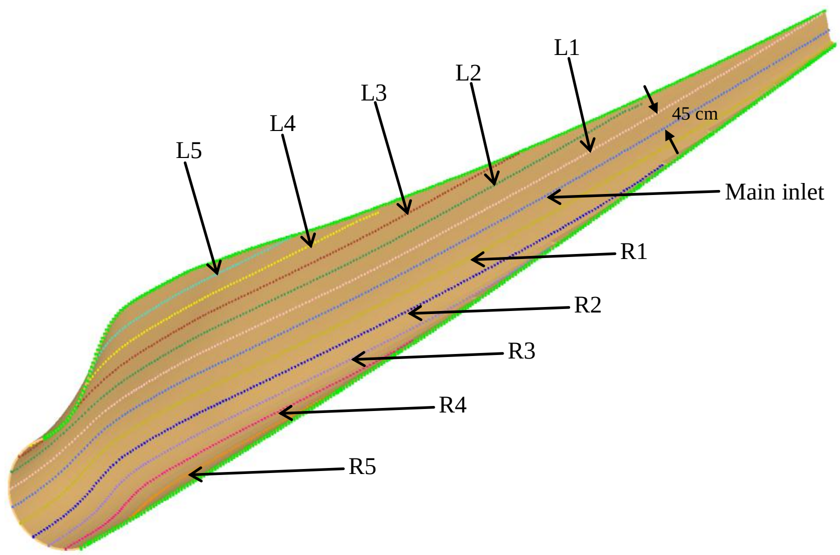

Figure 49. Inlet gate and outlet vents positioning for case 6.

In the case six, five auxiliary inlets were defined on each side of the main inlet gate with the same distance of 45 cm from each other (see figure 49). The optimum activation times and also the resulting filling times have been shown in table 5.

Table 5. Activation times and filling times for case 4.

Inlets	L1	L2	L3	L4	L5	R1	R2	R3	R4	R5	Filling time (Left)	Filling time (Right)
Activation times [s]	1,600	2,400	2,700	2,800	2,900	150	350	550	800	1,100	3,671 s	1,642 s

Selection of the optimum case

Figure 50 graphically shows the filling time associated to each case. It was shown that as the number of auxiliary gates increases from case to case, the filling time shortens in a parabolic trend and finally goes to a plateau after case five; therefore, it was concluded that further increasing the number of inlets can no longer be as effective on shortening the filling process.

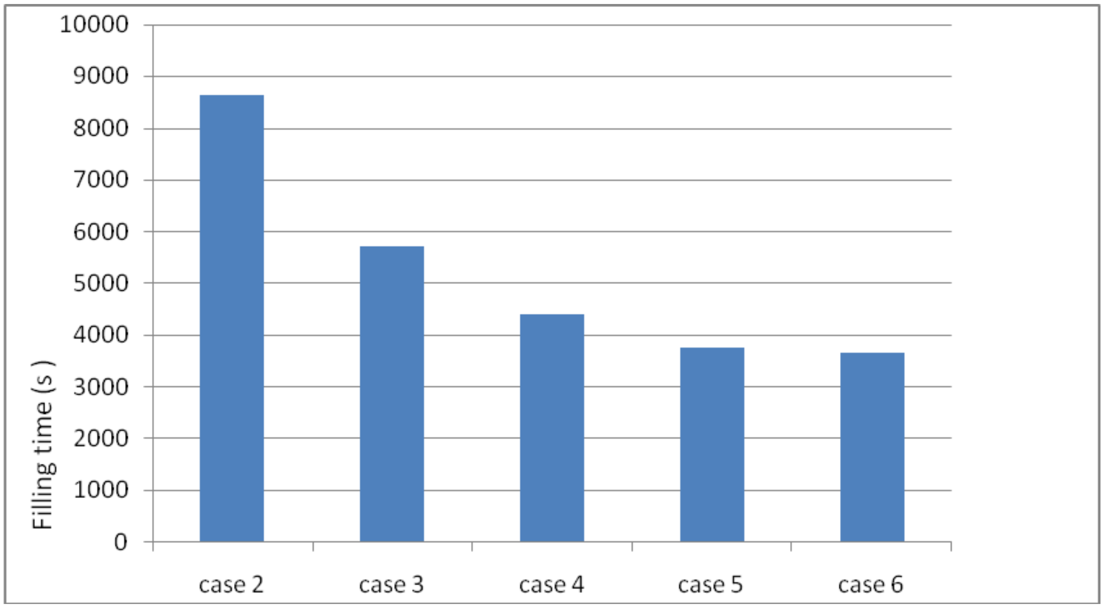

Figure 50. Filling times for all studied cases.

In order to choose a certain number of auxiliary gates as the optimum case, the effectiveness of the added inlets in shortening the process duration for each case had to be calculated. In Table 6 the first row shows the added length of inlet gate for each case compared to the previous case ,in the second row the resulted shortened filling time from the related previous case are shown and, the ratio of shortened time over the added length of inlet gate is shown in the third. The later value represents the effectiveness of the added inlets in shortening the process duration.

Table 6. The effectiveness of added inlet gates on shortening the filling process.

	Case 2	Case 3	Case 4	Case 5	Case 6
Added length of inlet compared to previous case (m)	29.7	28.8	24	26.2	30
Filling time Shortened, from the previous case (s)	-------	2,926	1,298	662	85
Filling time shortened by one meter of added inlet	-------	101.6	54.1	25.3	2.83

As it can be seen in Table 6, the shortened filling time by unit length of added inlet decreases by half from case to case, except for case six which it drops dramatically to about 10% of the one of case five; therefore the case six was drawn out and the case five was selected as the optimum case. However a more confident decision requires a tradeoff study based on detailed economic information on inlet costs and also on profits gained by shortening the filling process.

As it was discussed for case five; while four auxiliary inlets are used on the left side, using three inlets in the right is not only sufficient but it even manages to completes the filling process sooner than the left side. Therefore R4 auxiliary gate was removed while all activation times remained unchanged as indicated in the Table 9. By removing R4, the filling process on the right side took longer and it was completed after 2,774 seconds; as it was expected, the filling time in the left side remained the same.

References

[1] Berry, Derek. *Wind Turbine BladesManufacturing Improvements and Issues.* TPI Composites, Inc. February 24, 2004. http://www.sandia.gov/wind/2004BladeWorkshopPDFs /DerekBerry.pdf.

[2] Nolet, Stephen C. *Wind Turbine blades: Building Reliability.* TPI Composites, Inc. june 18, 2009. http://www.sandia.gov/wind/2009Reliability/PDFs/Day2-09-StephenNolet.pdf.

[3] M. S. Koefoed "Modeling and Simulation of the VARTM Process for Wind." *PhD Dissertation.* Aalborg University, 2003.

[4] Michael Bauccio, Ed. ASM International. *ASM Engineered Materials Reference Book.* Second Edition. Materials Park, OH, 1994.

[5] M. R. Kamal, S. Sourour. "Kinetics and thermal characterization of thermoset cure." *Polym.Eng.Sci.*, 1973: 59-64.

[6] Sun Suk Lee, Sung Chul Kim. "Analysis of unsaturated polyester-polyurethane interpenetrating polymer networks.I: reaction kinetics and viscosity model." *Polymer Engineering and Science*, 1991: 1182-1188.

[7] Dai-Soo Lee, Chang Dae Han. "A chemorheological model for the cure of unsaturated polyester resin ." *Polymer Engineering & Science* 27, no. 13 (July 1987): 955-963.

College of Engineering Wichita State University
Wind Energy Research Symposium

March 26th, 2009
1:00 – 5:00pm Room 307, NIAR

(www.wichita.edu/sustainability)

Supported by the Department of Energy (DOE DE-FG36-08GO88149)

Over the past year the College of Engineering has engaged in research activities that draw from aviation design and manufacturing research to target issues critical to the wide spread deployment of wind energy. This symposium will include presentations and posters summarizing the research and findings of faculty and students supported by a Department of Energy award.

Schedule of Presentations

Time	Topic	Presenter
1:00-1:20	Posters	Students
1:20-1:40	Welcome and Introductions	College of Engineering: Dean Zulma Toro-Ramos Project PI: Dr. Twomey
1:40-2:00	Network Monitoring and Control	Dr. Jewell
2:00-2:20	Wind Turbine Reliability and Maintainability	Dr. Steck
2:20-2:40	Environmental Impacts of Wind Energy Systems using Life Cycle	Dr. Overcash
2:40-3:00	Break/Posters	
3:00-3:20	Fiber-Reinforced Composite Blade UV Degradation Prevention using Nanotechnology	Dr. Asmatulu
3:20-3:40	Intelligent Manufacturing of Hybrid Carbon-Glass Fiber-Reinforced Composite Wind Turbine Blades	Dr. Minaie
4:00-4:20	Wind Energy Supply Chain/ Co-Generation Technologies (PEM Fuel Cells)	Drs. Yildirim and T.S. Ravi
4:20-4:30	Wrap-up	Dr. Twomey
	Posters	Students